analytical chemistry

pubs.acs.org/ac Article

Combined Liquid-State and Solid-State Nuclear Magnetic Resonance at Natural Abundance for Comparative Higher Order Structure Assessment in the Formulated-State of Biphasic Biopharmaceutics

Soumya Ranjan Pujahari, Pramod S. Mali, Rudra N. Purusottam, and Ashutosh Kumar*

Cite This: *Anal. Chem.* 2023, 95, 8469−8477 Read Online

ACCESS | Metrics & More | Article Recommendations | Supporting Information

ABSTRACT: A higher-order structure (HOS) is critical to a biopharmaceutical drug as the three-dimensional structure governs its function. Even the partial perturbation in the HOS of the drug can alter the biological efficiency and efficacy. Due to current limitations in analytical technologies, it is imperative to develop a protocol to characterize the HOS of biopharmaceuticals in the native formulated state. This becomes even more challenging for the suspension formulations where solution and solid phases coexist. Here, we have used a combinatorial approach using liquid (1D ^{1}H) and solid-state (^{13}C CP MAS) NMR methodology to demonstrate the HOS in the biphasic microcrystalline suspension drug in its formulated state. The data were further assessed by principal component analysis and Mahalanobis distance (D_M) calculation for quantitative assessment. This approach is sufficient to provide information regarding the protein HOS and the local dynamics of the molecule when combined with orthogonal techniques such as X-ray scattering. Our method can be an elegant tool to investigate batch-to-batch variation in the process of manufacture and storage as well as a biosimilarity comparison study for biphasic/microcrystalline suspension.

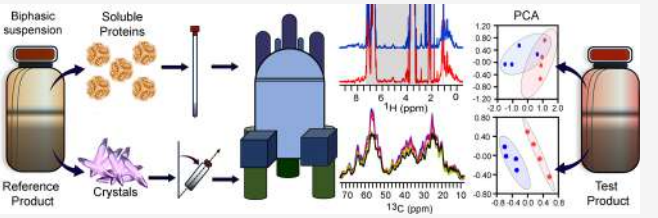

Low-volume, high-dose delivery of biotherapeutics is an emerging approach adopted by biopharmaceutical industries.[1] The monoclonal antibody is a significant class of biotherapeutics for treating many life-threatening diseases such as cancer, neurodegenerative diseases, diabetes, arthritis, etc., requiring high doses (>100 mg/mL) for the targeted delivery and optimum efficacy. Such highly concentrated drugs are formulated so that the lowest possible volume of the drug can be administered.[2] However, high doses of biotherapeutics are more prone to physical and chemical instability such as aggregation,[3] self-association,[4,5] liquid−liquid phase separation,[6−8] oxidation, and fragmentation[9,10] of the sample. Protein crystallization is the best possible approach to overcome such problems, which is less viscous than the solution formulation[11−13] of similar concentration,[14] is less prone to degradation, and has enhanced delivery pharmacokinetics over the solution formulation. Crystallization is also helpful in isolating and purifying proteins, enhancing biopharmaceutical manufacturability.[15,16] The crystallization of full-length mAbs appropriate for batch-scale manufacture and suitability for human administration has recently been a hot topic of research.[17,18] Insulin is currently the only biological product marketed as a microcrystalline (NPH formulation) and biphasic suspension formulation (mixture of suspension and soluble formulation). Insulin crystals preserve the higher order structure (HOS) state of insulin (hexamer).[19] The suspension portion exhibits prolonged protraction at the subcutaneous site and has a regulated release profile that mimics naturally released active insulin in the bloodstream.[20−22] Hence, the HOS of insulin, crystal morphology, crystal packing, crystallinity, and composition of the crystal are essential factors that can potentially impact the action profile of the suspension formulation.[23] The biphasic formulation satisfies both the bolus and basal requirements of insulin by virtue of soluble and suspension portions, respectively; it is of utmost importance to characterize insulin HOS in both formulations in their native state.

Protein HOS analysis is critical to understanding the molecular structure and defining biologics critical quality attributes. According to the International Conference on Harmonization Q6B guidelines, it is also essential for the test procedures and acceptance criteria for biological products.[24] Alteration in the HOS of the protein can impact the stability, quality, safety, and efficacy of biopharmaceutical products, leading to increased potential for immunogenicity and loss of biological function. Therefore, appropriate analytical tools are

Received: December 8, 2022
Accepted: April 24, 2023
Published: May 8, 2023

https://doi.org/10.1021/acs.analchem.2c05485
Anal. Chem. 2023, 95, 8469−8477

required to measure and monitor secondary, tertiary, and quaternary protein structures during early- and late-phase characterization and as part of comparability studies in the native formulated state. Several biophysical techniques are used regularly for biopharmaceutical characterization. For example, differential scanning calorimetry (DSC)[25] is used to monitor the phase transition of biomolecules, and Fourier transform infrared spectroscopy (FT-IR)[26] and circular dichroism(CD)[27] are used to decipher the secondary structure of proteins. While H/D exchange mass spectrometry (HDX-MS)[28] is helpful for peptide/protein fragment mass determination, X-ray diffraction,[25,29] liquid and solid-state nuclear magnetic resonance (NMR),[30,31] and cryo-electron microscopy (cryo-EM)[32] can elucidate three-dimensional global and local structure determination as well as drug−receptor interactions. Barring liquid-state NMR, biophysical techniques discussed above involve sample manipulation and may miss out on the native structure in its formulated state. NMR has several advantages over the others as it offers high structural resolution without any sample manipulation[33−35] and therefore is highly suited for characterizing biopharmaceuticals.

In this study, we have demonstrated an NMR-based approach that can be used for comparative assessment of the HOS for biphasic microcrystalline suspension biotherapeutics in its formulated state. Biphasic microcrystalline formulations are a combination of regular formulations (with soluble components) and microcrystalline proteins (insoluble components). Due to the colloidal biphasic nature, its characterization by established liquid-state NMR methods is not feasible, so we have used a combinatorial approach of liquid and solid-state NMR to investigate the biphasic suspension formulation. In our study, we separated the biphasic insulin drug into two fractions (solid and soluble) by centrifugation and carried out 1D ^{1}H liquid NMR and 1D ^{13}C CP-MAS NMR experiments for the soluble and solid fraction, respectively. For comparative assessment, the spectral outcomes from these experiments were further assessed using chemometric tools: principal component analysis (PCA) and Mahalanobis distance (D_M). In this study, we have used four batches each of marketed biphasic microcrystalline insulin suspension (Insulin 70/30 and Insulin 50/50) available in the Indian market branded as Huminsulin and Insugen. Eventually, we demonstrated that a combination of simple NMR methods and chemometric assessment could provide a high-resolution assessment of biphasic pharmaceutical suspensions that are not easily amenable to structural characterization in their native formulation states.

EXPERIMENTAL SECTION

Materials. All insulin microcrystalline biphasic drugs were purchased from the market. 10 mL of multiple-dose biphasic vial of each of Huminsulin 70/30 (100 IU/mL) and Huminsulin 50/50 (40 IU/mL) (*100 IU is not available), Insugen 70/30 (100 IU/mL) and Insugen 50/50(100 IU/mL) was used for the study (100 IU ∼ 3.5 mg equivalent of Insulin). Biphasic Insulin drugs are a mixture of regular insulin (water soluble) and microcrystalline (Neutral Protamine Hagedorn) formulation in different ratios (In 70/30, 70% microcrystalline and 30% soluble Insulin; similar in 50/50 both are in equal ratios). 10 mL of multiple-dose clear formulation of each Huminsulin R (100 IU/mL) and Insugen R (100 IU/mL) and microcrystalline (NPH formulation) of Huminsulin N was purchased over the counter [All Huminsulin products are from Eli Lilly (Indian marketed) and Insugen products are from Biocon Biologics Limited, Bengaluru, India]. Huminsulin and Insugen are independently approved generic drugs with similar insulin formulations with minuscule differences in the excipients. A Pierce BCA kit was purchased from Thermo Fischer Scientific, India.

Sample Preparation. ∼2 mL of sample was taken out from the vial by a syringe and separated into two fractions (soluble and solid fraction) by centrifugation at 500 g for 15−20 min. The solid fraction was transferred to a 1.9 mm ZrO_2 rotor by centrifugation with the same speed using a bench-top microcentrifuge device without further altering its native state. ∼4.5 mg of total crystalline protein was transferred to the rotor. ∼50% water content compared to the native formulated state was present inside the rotor. Epoxy glue was used to seal the top and bottom caps in order to maintain the hydration level and other volatile excipients' content. ∼500 μL of supernatant (soluble fraction) from the biphasic suspension was collected and transferred to a 5 mm NMR tube (Bruker) with 50 μL of D_2O for field locking without perturbing the formulation condition of the sample. The protein concentration of the soluble fraction was ∼1.05 and ∼1.75 mg/mL for 70/30 and 50/50 biphasic drugs, respectively.

NMR Spectroscopy. Solid-state and liquid-state NMR experiments were performed at 298 K (sample temperature) using a Bruker 750 MHz Avance III spectrometer connected with a variable temperature unit. Internal sample temperature was calibrated using sodium trimethylsilylpropanesulfonate (DSS) and was controlled using a variable temperature unit. Topspin 3.6.2 pl6 and Topspin 4.1.0 Bruker NMR software were used for data acquisition and processing. All liquid-state NMR experiments were performed with a triple resonance (TXI) room-temperature (RT) probe. 1D ^{1}H NMR spectra were acquired using a standard Bruker pulse program ('zgesgp') with a recycling delay of 1 s. As the sample concentrations were very low, 4 k scans were collected with an experimental time of ∼3 h. All data were processed with an exponential multiplication window function with 3 Hz line broadening.

Solid-state NMR experiments were carried out on a 1.9 mm HCN triple resonance probe, and for better sensitivity, it was configured to double resonance mode. The 1D ^{13}C Cross-polarization magic angle spinning (CP-MAS)[36] experiment was performed with an optimized cross-polarization (CP) contact time of ∼1.25 ms and a ramp of 100−70% on the spin-lock radio frequency (RF) power. A typical ^{1}H 90° pulse RF of power 137 kHz was used. During ^{13}C acquisition of up to 21.7 ms, the ^{1}H RF power of the phase-inverted supercycled sequence for attenuation of rotary resonance (PISSARRO)[37] decoupling scheme was set to 137 kHz. The recycle delay was kept for 3 s with an experimental time of ∼2.5 h with a number of scans of 3072. Sample processing was done using the window function (exponential multiplication) with a line broadening of 100 Hz. The line broadening can be reduced to 50−80 Hz depending on the spectra with a higher signal-to-noise ratio. However, noise may interfere during the PCA if lesser line broadening is kept for those cases where S/N is not appreciable. Therefore, a line broadening of 100 Hz was kept to maintain uniformity. For the CP build-up experiment, a series of 1D ^{13}C CP-MAS NMR spectra with variable cross polarization contact time ranging from 10 to 1400 μs were recorded for each representative batch of Insugen 70/30 and Huminsulin 70/30. The intensity integrals of the aliphatic

https://doi.org/10.1021/acs.analchem.2c05485
Anal. Chem. 2023, 95, 8469−8477

region (10−70 ppm) of the 1D ^{13}C CP-MAS NMR spectra of both I 70/30 and H 70/30 were normalized, and the spectra were plotted against the CP contact time to obtain the hC-CP build-up curve.

2D ^{13}C-^{1}H HETCOR was recorded with a CP contact time of ∼1.25 and ∼0.3 ms for ^{1}H to ^{13}C and ^{13}C to ^{1}H CP steps, respectively, with a ramp of 70−100% on the spin-lock RF power at a Magic Angle Spinning (MAS) frequency of 33 kHz. We used ∼80 to 60 kHz of ^{1}H and 60−40 kHz ramp power to establish Hartmann−Hahn matching conditions and a proton decoupling power of ∼100 kHz during acquisition with a recycle delay of 1.5 s. The number of scans used was 480, with 512 and 256 data points in direct (^{1}H) and indirect (^{13}C) dimensions, respectively, with an acquisition time of 4.91 ms for an experimental time of ∼31 h.

Principal Component Analysis. PCA was performed separately for both liquid (1D ^{1}H) and solid (^{13}C CP-MAS) state NMR spectra by using Mestronova 14.2.3 software. Spectra of four different batches of each drug class were grouped into separate classes. For the 1D ^{1}H spectra, corresponding resonance peaks for the excipients, buffer components, and water (1.044−1.137, 1.80−7.37, 9.13−10.00 ppm) were excluded from the PCA calculations. All the regions taken for PCA calculations were binned with 0.02 ppm with summed spectral intensities in each bin. The summed intensities were processed with integrity check, filtered with Inter quartile range (25%), normalized, and Pareta-scaled before PCA.

Similarly, for ^{13}C CP-MAS NMR spectra resonance peaks corresponding to aliphatic, aromatic, and carbonyl regions were considered for PCA calculation, remaining regions (0.00−10.3, 73.5−111.0, 140−153.4, 161.5−168.3, 181.0−200.0 ppm) were excluded. All the regions taken for PCA calculations were binned with 0.4 ppm resolution with summed spectral intensities in each bin. The summed intensities were processed with integrity check, filtered with inter quartile range (25%), normalized, and Pareta-scaled before PCA calculation.

Mahalanobis Distance Calculation. The Mahalanobis distance was calculated using PC scores from the PCA as discussed by Wang et al.[38] A sample matrix was made for each drug of interest for the comparison, where rows correspond to the total number of batches and columns denote the total number of Principal Components (PC). We have taken four different batches of each drug for our calculation. Three PC components were taken for 1D ^{1}H spectra and five components were considered for ^{13}C CP-MAS spectra. The covariance matrix and the Mean vector for each sample matrix were calculated. The following formula calculated the Mahalanobis Distance.

$$D_M = \sqrt{(A_. - B_.)S^{-1}(A_. - B_.)'}$$

where D_M denotes the Mahalanobis distance, $\overline{A}$ and $\overline{B}$ denote the mean vector of the sample matrix (A and B), and S denotes the average covariance matrix of both samples matrix.$(\overline{A} - \overline{B})'$denotes the transpose matrix of $(\overline{A} - \overline{B})$.

Crystal Morphology Study by Bright Field Microscopy. 2 μL of the drug was placed in a glass slide in its native formulation. Coverslips were mounted above the sample, followed by immersion oil. The crystal images were captured under a laser scanning microscope (Carl Zeiss, LSM 780) with 60X zoom. We measured the length of 100 crystals from each drug and plotted it in a Gaussian distribution using Image J and OriginPro (2021) software, respectively.

Wide-Angle X-ray Scattering (WAXS). WAXS data for Insugen 70/30 and Huminsulin 70/30 were collected at Xenocs 2.0 SAS instrument using an Eiger R1M vacuum fed through a set high-resolution hybrid pixel photon-counting detector. Samples were transferred to a capillary tube and kept at 4 °C overnight to settle the crystals. The X-ray scattering pattern was collected from the bottom of the capillary after exposure for 2 h at room temperature. The distance between the sample and detector was 333.307 mm, and the range of scattering angle (2θ) 1.5−5° was covered. The buffer scattering was subtracted from the original crystal scattering. OriginPro (2021) software was used for data processing and plotting.

Invitro Release of Insulin from the Crystal. The release of the insulin hexamer from crystals was observed for 13 h. 2 mL of each sample was centrifuged, and crystals were collected after the supernatant was discarded. Crystals were dissolved in 25 mL of release buffer (50 mill molar phosphate buffer, pH 7.4 with 0.01% tween-80) in a 50 mL falcon tube at 37 °C and shaken at 50 rpm in an incubator. 25 μL of aliquot were taken out in triplicate and mixed with 200 μL of working BCA reagent, and absorbance of the mixture (copper-BCA complex) was recorded at 562 nm after 3 and 13 h. The insulin standard curve was made by plotting the known concentrations of insulin against its absorbance at 562 nm (Figure S6.) All the experiments were carried out in triplicate, and a statistical t-test was performed by using origin pro (2021) software.

RESULTS AND DISCUSSION

Human insulin in the biphasic microcrystalline suspension (dispersed microcrystalline solid in a liquid) drug exists in the hexameric state in the presence of metal ion Zinc and m-cresol, which has been well established through X-ray crystallography.[19] While the hexameric state enhances the stability of insulin, the microcrystalline suspension formed due to protamine sulfate leads to the protracted release of insulin. Nonetheless, the monomeric state of insulin is biologically active and participates in its functional activity (Figure 1A).

HOS characterization of biphasic microcrystalline in the formulated state is challenging as the formulation exists in soluble and insoluble fractions. Also, the solid fraction (microcrystalline protein) settles down, leaving the soluble fraction as a supernatant when the formulation is kept for 10−15 min. We exploited this property and made the process easier; we separated both fractions by mild centrifugation. The soluble formulation of Insulin is known to preserve the hexameric state of the insulin in the presence of zinc and m-cresol. The 1D ^{1}H spectra of the soluble fraction of Huminsulin 70/30 were compared with the intact biphasic suspension without any perturbation to investigate any possible impact on higher-order protein structure during the separation of the two components. We found no differences in the spectral distribution in methyl and amide regions indicating, the HOS in the soluble fraction is well preserved after the separation by centrifugation (Figure S1).

Furthermore, we assess the water content of the crystalline fraction inside the rotor as the hydration level plays a crucial role in maintaining the crystalline structure. We performed 1D ^{13}C CP-MAS for native NPH formulation (100% crystalline) without centrifugation and compared the spectral quality in different hydration levels for Huminsulin (Figure S2). For

https://doi.org/10.1021/acs.analchem.2c05485
Anal. Chem. 2023, 95, 8469−8477

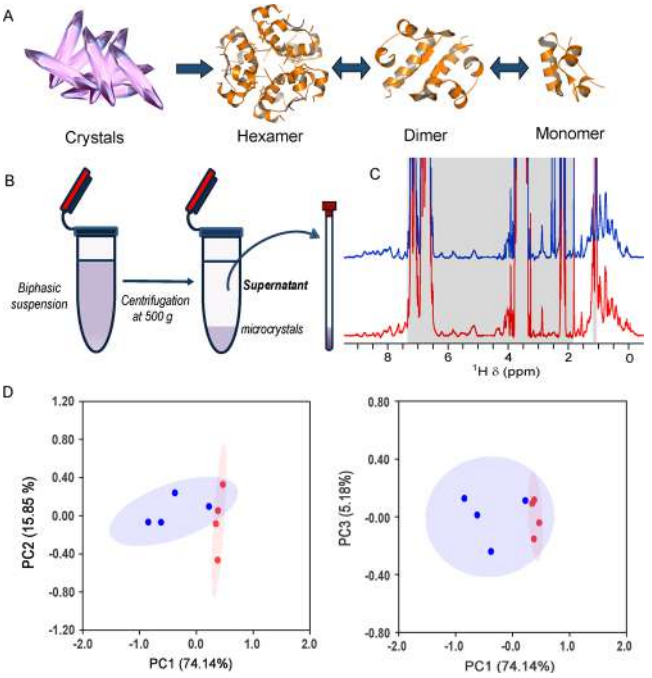

Figure 1. (A) Cartoon mimicking insulin hexamer releases from the crystal, which further converts to dimer and monomer (active form). (B) Schematic of higher order structural similarity comparison of soluble fractions of the biphasic suspension by 1D ^{1}H NMR spectroscopy. (C) 1D ^{1}H NMR spectra of soluble fraction of Huminsulin 70/30 (red) stacked with soluble fraction of Insugen 70/30 (blue). PCA calculation was carried out for aliphatic and amide regions. The excipients (shaded in gray) spectra were excluded from the calculation. (D) Score plot of principal component 1 (PC1) vs principal component 2 (PC2) and principal component 1 (PC1) vs principal component 3 (PC3) of the soluble fraction of Huminsulin 70/30 (orange) and soluble fraction of Insugen 70/30 (blue). Blue and red ellipses are drawn with 95% CI for Insugen and Huminsulin, respectively.

native NPH formulation, the water content was considered to be 100%, and the protein content inside the rotor was ∼40 μg. We recorded a 30 K scan and can achieve an S/N ratio of only 1.5. However, we believe that it may not be a commercially viable option to perform such an analysis in the native state at natural abundance due to low S/N. We further concentrated the crystalline part by mild centrifugation and made it to 80% and 50% relative hydration levels compared to the native formulation inside the rotor. Clearly, a better S/N was observed for these samples. At 50% relative hydration, we observed good S/N with a value of >10 in a reasonable experimental time of ∼2.5 h, which is typically required during the quality assessment of pharmaceuticals. Except for better resolution and sensitivity, spectra were found to be comparable at different hydration levels, indicating that our choice of 50% hydration is optimal. It does not impede the crystalline structure of the native formulated state; therefore, we carried out all our experiments with 50% of relative hydration to the native formulated state.

HOS Assessment for the Soluble Fraction of the Insulin Biphasic Formulation. 1D ^{1}H NMR is a high-resolution technique that provides valuable information about the overall protein structure and its folded state. Bramham et al. have shown the usefulness of 1D ^{1}H NMR to investigate the stability of protein and excipients in the native biopharmaceutical formulation.[39] However, 1D ^{1}H NMR is limited to biopharmaceuticals in a solution formulation. Typically, crystalline suspensions are converted to soluble states to investigate using liquid-state NMR, which might introduce structural perturbation, whereas, in this study, because of the biphasic nature, the soluble and solid fractions of the biphasic microcrystalline formulation were separated by mild centrifugation without perturbing the native state (Figure 1B) and were assessed independently by liquid and solid-state NMR, respectively.

1D ^{1}H NMR on the soluble fraction (SF) of Huminsulin 70/30 (H 70/30) and Insugen 70/30 (I 70/30) was performed (Figure 1C). A good spectral dispersion (∼3 ppm) was observed in the amide region, indicative of a well-folded protein. The spectral fingerprint in the methyl and amide regions was comparable between the two drug products. Though qualitative comparison was informative, we performed PCA for quantitative assessment. PCA is a well-established chemometric approach often used for comparability assessment of biotheraputics.[38] For PCA calculations, we recorded 1D ^{1}H NMR for four different lots of each drug product. To overcome any impact of firm excipients peaks, spectral regions only specific to human insulin peaks were considered for the PCA analysis. The first three PC components accounted for >90% of spectral variations. PCA score plots between SF of H 70/30 and SF of I 70/30 (Figure 1D) showed a promising cluster similarity. Using these PC scores, Mahalanobis Distance (D_M) was calculated, and it was found to be 2.69. Considering D_M of 3.3 as an acceptance similarity metric criterion; for many regulatory agencies (e.g., FDA, EMA), also shown by Wang et al.,[38] both drug products showed a comparable higher order structure between Insugen 70/30 and Huminsulin 70/30 in the soluble fractions. A similar study was performed with the Insugen 50/50 and Huminsulin 50/50 (Figure S3), and the results were similar to the above.

HOS Assessment for the Suspension Fraction of the Insulin Biphasic Formulation. 1D ^{13}C CP-MAS NMR is a powerful noninvasive, nondestructive structural characterization tool for samples observed at natural abundance, most beneficial for biopharmaceutical samples,[40] where isotope labeling of samples is challenging. A previous study by Li et al. investigated the crystallinity and crystal stability of microcrystalline pembrolizumab upon dehydration and change in temperature by using MAS NMR.[40]

We carried out all solid experiments with ∼50% hydration level of the native formulation for a better S/N ratio and minimum possible experimental time. The initial set of experiments was carried out to assess the suitability of lower MAS rates for more commonly available MAS rotors for routine assessment in drug quality control. We conducted a comparative study of 1D ^{13}C CP MAS experiments at different MAS rates of 20 and 33 kHz. At 33 kHz, the spectral peaks were a little sharper compared to 20 kHz; however, we did not observe significant differences in the linewidth of the spectra at both spinning speeds (Figure S5). Considering the higher availability of lower MAS rates rotors in drug quality control, we suggest a spinning speed of 20 kHz suffices to investigate the molecular level structural details and dynamics of a suspension formulation of molecules ranging from small proteins up to 40 kDa. (Insulin hexamer ∼36 kDa).

As discussed above, for the suspension portion containing microcrystalline particles (Figure 2A), we performed 1D ^{13}C cross-polarization at an MAS rate of 20 kHz for structural

https://doi.org/10.1021/acs.analchem.2c05485
Anal. Chem. 2023, 95, 8469−8477

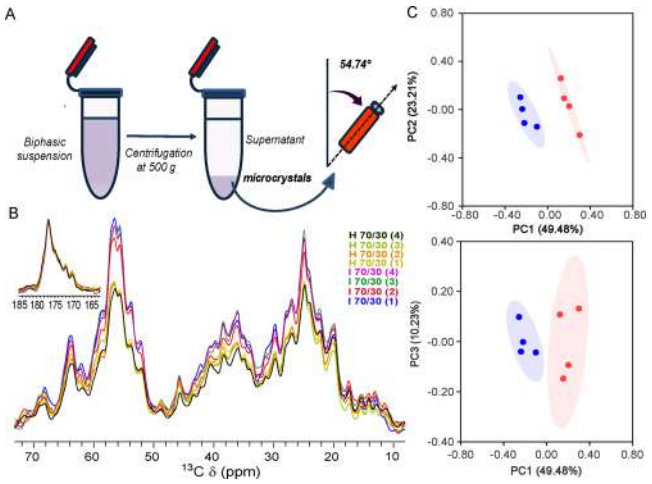

Figure 2. (A) Schematic of higher order structural similarity comparison of solid fractions of the biphasic suspension by 1D ^{13}C CP-MAS NMR. (B) All four 1D ^{13}C CP-MAS NMR spectra of the solid fraction of Insugen 70/30 (blue, red, green, magenta) superimposed with a solid fraction of Huminsulin 70/30 (yellow, orange, light green, dark green). The carbonyl region of all the spectra was normalized, as shown in the small inset. (C) Score plot of principal component 1 (PC1) vs principal component 2 (PC2) and principal component 1 (PC1) vs principal component 3 (PC3) of the solid fraction of Insugen 70/30 (blue) and solid fraction of Huminsulin 70/30 (orange). Blue and red ellipses are drawn with 95% CI for Insugen and Huminsulin, respectively. Full-length spectra are provided in the Supporting Material.

assessment. The qualitative assessment of overlaid spectra of 1D ^{13}C CP MAS showed a high degree of fingerprint match between both drug products, suggesting that the HOS structure of insulin inside the crystals is highly similar. However, in the aliphatic region of the spectra, we could observe an intensity difference (when the carbonyl regions were normalized) (Figure 2B). Furthermore, we recorded four different batches of each drug product. As specified above, regions specific to aliphatic, aromatic, and carbonyl peaks were selected for PCA calculations, followed by Mahalanobis distance calculation.[38] Unlike the soluble fraction, the PCA plots did not show any overlap (Figure 2C), and the Mahalanobis distance (D_M) for the suspension fraction was found to be 40.83, clearly showing the differences in the two drug products. A similar study on the 50/50 biphasic drug yielded a D_M value of 117.22, indicating differences in the two sets of samples (Figure S4). To verify the difference in the PCA and high D_M values only because of the difference in intensity in the aliphatic region, we replicated the study in the crystalline protein of the same brand (as control) between Huminsulin 70/30 and Huminsulin 50/50 and interestingly observed no differences in the spectral pattern as well as the intensity in the aliphatic region. The PC plots were found well overlapped with each other, and the D_M value was found to be 2.52, suggesting that there are no differences in the drug products (Figure S7).

The intensity of the aliphatic region of Huminsulin 70/30 was less compared to Insugen 70/30. As the CP dipolar coupling transfer is directly proportional to the molecule's rigidity, it indicates that the aliphatic region of Huminsulin batches is more flexible than the Insugen, resulting in less CP transfer. To further validate this observation, we recorded a series of 1D ^{13}C CP MAS experiments with variable CP contact time (ranging from 10 to 1400 μs) to obtain the hC-CP build curve. The intensity integrals of the aliphatic region (10−70 ppm) were normalized and plotted against the CP contact time for both Insugen 70/30 and Huminsulin 70/30. We observed a marginally faster build-up curve with oscillation for I 70/30. The CP build-up reaches the maximum intensity earlier in I 70/30 (400 μs) compared to H 70/30 (600 μs) (Figure 3A,B). It is well established that if there is dominant dipolar interaction, the polarization transfer shows oscillatory behavior.[41,42] The frequency of transient oscillation is directly proportional to the dipolar coupling constant, which reflects the mobility or rigidity of nuclei involved therein.[43] A higher transient oscillation is directly proportional to the rigidity of the molecule.[42,44] Higher oscillation in the build-up curve suggested that nuclei in I 70/30 are relatively more rigid compared to H70/30. The correlation of chemical shift and heteronuclear dipolar coupling interactions has been studied using pulse sequence such as polarization inversion spin exchange at the magic angle (PISEMA)[45] to determine the peptide structure in an oriented membrane. Similarly, several studies used different modes of magnetization transfer, such as dipolar-coupling-based or J-coupling-based mechanisms for spectral editing for the rigid or flexible part of the protein.[46] To further investigate any differences in the quality of the two drug products and delineate the origin of the difference appearing in various formulations, we performed additional assessment by 2D ^{1} ^{13}C-^{1}H HETCOR NMR (ssNMR) and WAXS on a representative batch of the two products.

2D ^{13}C-^{1}H HETCOR Spectral Comparison. In 1D CP MAS experiments, resolution in the carbon dimension was limited, which could be overcome by recording 2D (^{13}C,^{1}H) correlation spectra. Due to higher sensitivity, ^{1}H is the preferred nucleus of detection; therefore, we used a proton-detected ^{13}C-^{1}H 2D heteronuclear correlation (HETCOR)[47]experiment with improved resolution. Such experiments have been performed on insulin[48] and mAbs[40] to gain structural insights into these classes of formulated biopharmaceuticals.

From the 2D ^{13}C-^{1}H HETCOR spectral comparison, we did not observe a significant difference in the two spectra. However, we could even see that CP transfer around 25 ppm (methyl's) is significantly higher for ^{13}C resonances. This resulted in the appearance of more peaks and the spectral resolution in the methyl region and Cα region (50−70 ppm) in the w_1 (^{13}C) dimension for the I 70/30 (Figure 4C,D) than H 70/30 (Figure 4E,F). This also corroborated with the observation from the 1D ^{13}C CP MAS spectra. From all the above experiments, we observed that insulin molecules present in I 70/30 are more rigid compared to H 70/30 in the crystal lattice, allowing efficient CP transfer in the side chains of the amino acids. This could potentially be due to slightly different packing in its crystalline state. We hypothesized that the number of insulin molecules in one-unit crystal area is more in the case of I 70/30, making the crystal packing more compact than H 70/30 (Figure 3G,H). We carried out WAXS experiments for both microcrystals to further verify our speculation on crystal packing.

Characterization of Microcrystals through WAXS. X-ray crystallography is a well-established technique extensively used for investigating protein microcrystals.[19] Balschmidt et al. have shown the preparation of the Neutral Protamine Hagedorn (NPH) formulation of the insulin hexamer containing two zinc atoms and one protamine molecule at

https://doi.org/10.1021/acs.analchem.2c05485
Anal. Chem. 2023, 95, 8469−8477

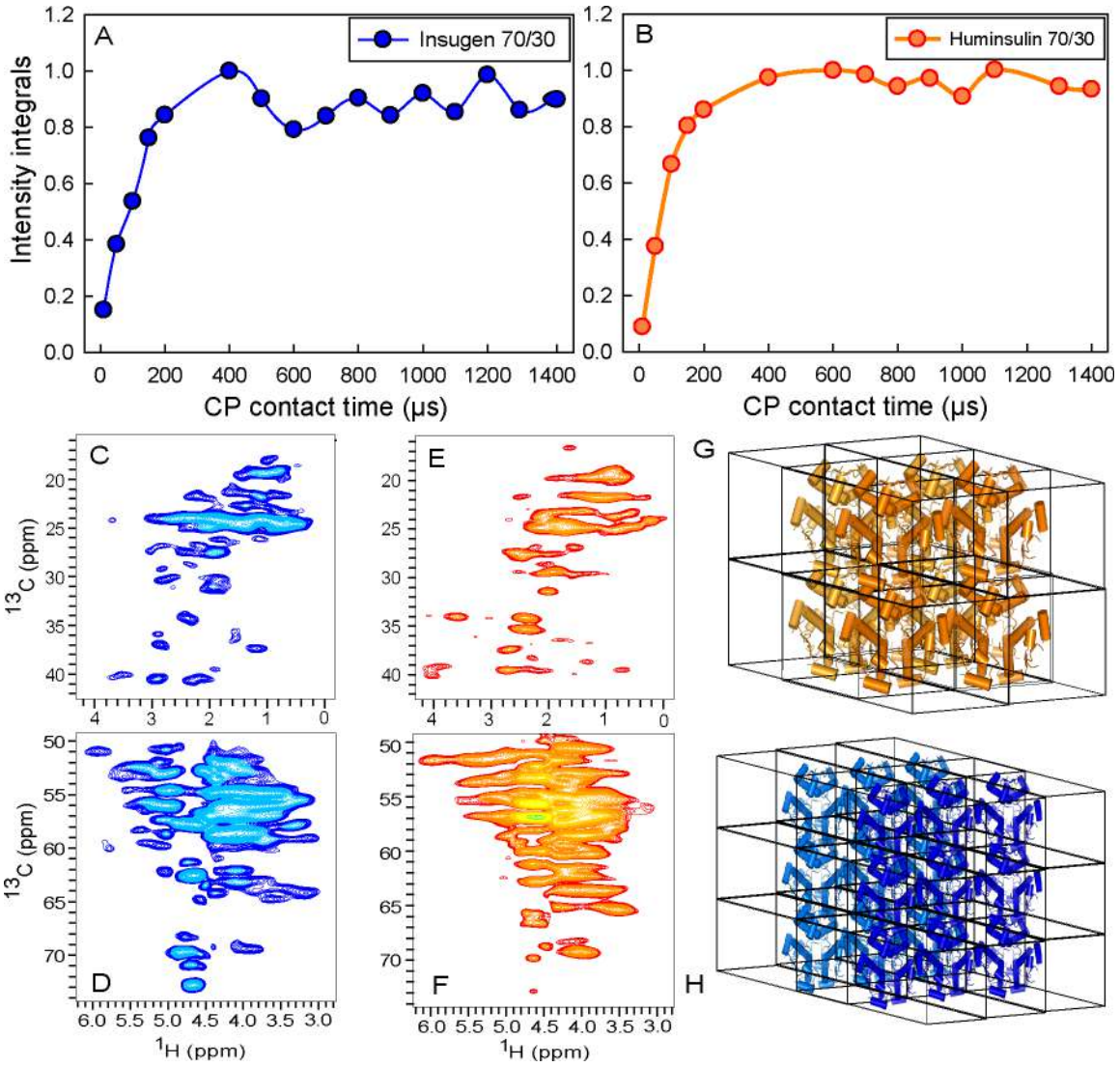

Figure 3. hC-CP build-up curve of aliphatic regions (10−70 ppm) of the solid fraction of Insugen 70/30 (A) and Huminsulin 70/30 (B). 2D ^{13}C-^{1}H CP MAS HETCOR spectra of Insugen 70/30 (C, D) vs Huminsulin 70/30 (E, F). Schematic of the packing of insulin in the crystallite, showing more compactly packed in I 70/30 (H) and corporately loosely packed in H 70/30 (G).

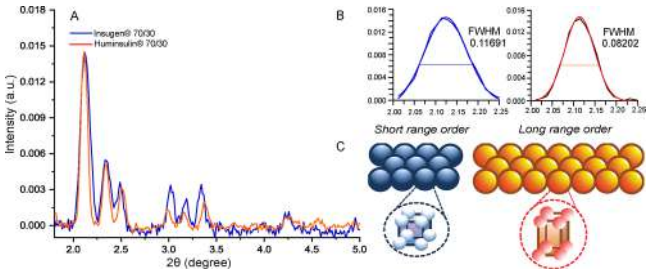

Figure 4. (A) Comparison of the diffraction pattern of Huminsulin 70/30 and Insugen 70/30 crystals (spectral intensities were normalized). (B) Comparison of the FWHM at peak 2.12° of I 70/30 (blue) and H 70/30 (orange). (C) Comparison of the range order of crystallite packing, which was found short-range order and long-range order for I 70/30 (blue) and H 70/30 (orange), respectively.

pH 7.3 in the tetragonal crystal system (space group $p4_32_12$).[49] However, X-ray diffraction on a single crystal of a biopharmaceutical sample is very difficult due to the smaller size. In a study, Norrman et al, performed an X-ray diffraction study of different commercial and in-house insulin microcrystalline formulations by using a synchrotron.[50]

We recorded scattering profiles from angles ranging from 1.5 to 5° for I 70/30 and H 70/30 microcrystals. Multiple characteristic peaks at approximately similar 2θ values were found for both samples, suggesting that both the crystals are made up of unit cells of a similar spacegroup[50](Figure 4A). However, further analysis of the first-order Bragg peaks (which are centered at 2θ = 2.12 for both the samples) provided a FWHM of 0.11691 and 0.08202 for I 70/30 and H 70/30, respectively (Figure 4B). This indicated a difference in the long-range order of the crystals in both samples. Now, the Debye−Scherrer analysis[51] of the Bragg peaks can be used to obtain the crystallite size (D) viz. the long-range order in the material and is given by $D = K\lambda/(\beta \cos \theta)$, where K is Scherrer's constant (K = 0.94), λ is the X-ray wavelength (1.54 Å), β is FWHM of the diffraction peak, and θ is the diffraction angle. Accordingly, the crystallite size for I 70/30 and H 70/30 was 12.39 and 17.67 nm, respectively (see the Supporting Information for calculation). This suggested that although the crystal was of a similar space group, the H 70/30 exhibited a

https://doi.org/10.1021/acs.analchem.2c05485
Anal. Chem. 2023, 95, 8469−8477

higher long-range order as compared to I 70/30 (Figure 4C). Furthermore, the FWHM of the subsequent peaks follows a similar trend, confirming the higher long-range order of H70/30 (Table S4). Higher order Bragg peaks (in the range 2θ = 2.4−3.5°) for I 70/30 and H 70/30 showed a slight deviation in the peak maxima, suggesting the difference in the unit cell lengths although the space group remained similar (Figure 4C). This is in agreement with the previously reported studies on insulin crystals.[50] Thus, the spatial arrangement of the insulin hexamer in I 70/30 is close to each other (as the length of the unit cell is shorter) inside the unit cell of the crystal and makes it more compact compared to H 70/30. The observations stemming from WAXS and ssNMR corroborated sufficiently well and suggested a difference in the level of the crystal packing of the microcrystalline formulation.

Crystal Morphology Study and Invitro Release of Insulin from the Crystal. Microcrystalline suspension of insulin is prepared for sustained release of the drug. The dissolution of the crystal plays a rate-limiting factor in the absorption of the drug into the blood stream.[50] Thus, careful investigation of the physical and chemical properties of the crystals is needed to maintain the homogeneity of the crystalline formulation. As we observed the difference in the crystal packing, we investigated the morphology of the crystals using bright field microscopy. We found similar crystal morphology, long and pointed-ended (Figure 5A,B), and a

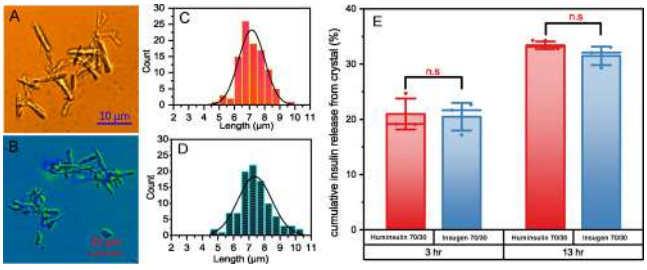

Figure 5. Comparison of the insulin crystal size of H 70/30 (A) and I 70/30 (B) by bright-field microscopy. The length of 100 insulin crystals from each drug was measured, and a graph was plotted between the length of the crystal (*X*-axis) and the number of counts (*Y*-axis). The length of Huminsulin 70/30 (C) was found in the range of 5−9 μm, and Insugen 70/30 (D) was in the range of 5.5−10 μm. (E) Release of insulin from the crystal was observed for 3 and 13 h in release buffer (phosphate buffer pH 7.4, with 0.01% of tween-80), and a t-test was performed and found no significant difference in both cases.

size distribution of 5−9 μm for both H 70/30 and I 70/30 (Figure 5C,D). The differences in the crystal packing could also impact the kinetics of the dissolution of the insulin molecule from the crystal; therefore, we performed an invitro Insulin release assay of the microcrystalline formulation. From the invitro insulin release study, we found a similar cumulative percentage of Insulin released out from the crystals at 3 h (∼20%) and 13 h (∼33%) (Figure 5E).

The release of insulin from the crystals under laboratory conditions is comparatively slow. In physiological conditions, enzymes and proteases play a role in the faster release of insulin from the crystals.[22] Nonetheless, despite having differences in the crystal packing, we could not observe any significant difference in the release of protein from the crystal for both drug products.

To further assess if the differences in the crystal packing have led to perturbation in the active state of Insulin (monomer), we performed a structural assessment of acidified samples of both drug products. For this, the sample pH was adjusted to 2.3. Next, 1D ^{1}H and 2D ^{1}H-^{13}C SOFAST methyl HMQC NMR were recorded (Figure S11). Insulin is known to exist in its monomeric state at lower pH. Both drug products showed a highly comparable spectral profile indicating highly similar monomeric (active) conformation. While variations in the crystal packing, as observed by ssNMR and WAXS studies, did not show any direct impact on its functionally active state or release, it may have an impact on the long-term storage of the samples. Insulin biphasic suspension products are marketed as multidosage vials/pens and can be stored at ambient temperature during the actual usage of typically ∼30 days. At ambient temperature, crystal packing differences may lead to differences in the degradation kinetics; hence, it is important to have appropriate monitoring and control during the manufacturing of suspension formulations.

CONCLUSIONS

In this work, we have proposed a combinatorial approach for higher-order structure similarity comparison for biphasic microcrystalline suspension in its formulated state. We separated the soluble and solid fractions from the biphasic microcrystalline formulation and performed 1D ^{1}H liquid and 1D ^{13}C CP-MAS NMR spectra for both solution (30% part) and the suspension (70% part) part, respectively. For qualitative HOS assessment, we compare the 1D NMR spectra independently for both solution and a solid fraction, followed by PCA and Mahalanobis distance for quantitative assessment. 2D HETCOR experiments did not provide any critical information due to low concentration and low resolution for the solution and solid fractions, respectively. Also, 1D ^{13}C CP-MAS NMR spectra were sufficient to provide information regarding the rigidity of the molecule (confirmed via hC-CP build-up curves) and crystal packing (corroborates data from WAXS) which is reflected by the intensity differences in the CP transfer. Therefore, we strongly suggest that a combination of 1D ^{1} H liquid NMR and 1D ^{13} C CP MAS NMR experiments is an elegant tool to compare the HOS and dynamics of the biphasic/microcrystalline suspension formulation.

ASSOCIATED CONTENT

Supporting Information

The Supporting Information is available free of charge at https://pubs.acs.org/doi/10.1021/acs.analchem.2c05485.

Similar comparative study of Huminsulin 50/50 and Insugen 50/50, CP MAS spectral comparison at different spinning speeds, standard curve for insulin release, and comparison study of the insulin monomer (PDF)

AUTHOR INFORMATION

Corresponding Author

Ashutosh Kumar − *Department of Biosciences and Bioengineering, IIT Bombay, Mumbai 400076, India;* orcid.org/0000-0002-5061-8162; Phone: 0091-22-25767762; Email: ashutoshk@iitb.ac.in, ashutosh.nmr@gmail.com; Fax: 0091-22-25767771

https://doi.org/10.1021/acs.analchem.2c05485
Anal. Chem. 2023, 95, 8469−8477

Authors

Soumya Ranjan Pujahari − *Department of Biosciences and Bioengineering, IIT Bombay, Mumbai 400076, India;* orcid.org/0000-0002-0739-1732

Pramod S. Mali − *Department of Biosciences and Bioengineering, IIT Bombay, Mumbai 400076, India;* orcid.org/0000-0002-8205-2044

Rudra N. Purusottam − *Department of Biosciences and Bioengineering, IIT Bombay, Mumbai 400076, India*

Complete contact information is available at: https://pubs.acs.org/10.1021/acs.analchem.2c05485

Author Contributions

S.R.P. contributed by proposing the idea, designing experiments, performing experiments and data analysis, and writing the manuscripts. P.S.M. and R.N.P. contributed by setting up NMR experiments and proof reading of the manuscript. A.K. contributed in conceptualization, reviewing and editing the manuscript, and supervising the experiments performed.

Notes

The authors declare no competing financial interest.

■ ACKNOWLEDGMENTS

This work has been supported by HFNMR 750 MHz, microscopy and WAXS facility, funded by RIFC, IRCC, DST-SAIF, and IIT Bombay. We acknowledge CSIR for primary financial support. Financial support for this project was also received from IRCC and Technocraft Centre for Applied Artificial Intelligence (TCA2I), IIT Bombay. We thank Prof. Kamendra sharma for the useful inputs in the analysis of WAXS data. We also thank Mr. Gokulakrishnan M for helping in making figures.

■ REFERENCES

(1) Mathaes, R.; Koulov, A.; Joerg, S.; Mahler, H.-C. *J. Pharm. Sci.* **2016**, *105*, 2255−2259.
(2) Jackisch, C.; Müller, V.; Maintz, C.; Hell, S.; Ataseven, B. *Geburtshilfe Frauenheilkd.* **2014**, *74*, 343−349.
(3) Joubert, M. K.; Luo, Q.; Nashed-Samuel, Y.; Wypych, J.; Narhi, L. O. *J. Biol. Chem.* **2011**, *286*, 25118−25133.
(4) Liu, J.; Nguyen, M. D. H.; Andya, J. D.; Shire, S. J. *J. Pharm. Sci.* **2005**, *94*, 1928−1940.
(5) Lilyestrom, W. G.; Yadav, S.; Shire, S. J.; Scherer, T. M. *J. Phys. Chem. B* **2013**, *117*, 6373−6384.
(6) Luo, H.; Lee, N.; Wang, X.; Li, Y.; Schmelzer, A.; Hunter, A. K.; Pabst, T.; Wang, W. K. *J. Chromatogr. A* **2017**, *1488*, 57−67.
(7) Nishi, H.; Miyajima, M.; Nakagami, H.; Noda, M.; Uchiyama, S.; Fukui, K. *Pharm. Res.* **2010**, *27*, 1348−1360.
(8) Reiche, K.; Hartl, J.; Blume, A.; Garidel, P. *Biophys. Chem.* **2017**, *220*, 7−19.
(9) Cohen, S. L.; Price, C.; Vlasak, J. *J. Am. Chem. Soc.* **2007**, *129*, 6976−6977.
(10) Moritz, B.; Stracke, J. O. *Electrophoresis* **2017**, *38*, 769−785.
(11) Basu, S. K.; Govardhan, C. P.; Jung, C. W.; Margolin, A. L. *Expert Opin. Biol. Ther.* **2004**, *4*, 301−317.
(12) Merkle, H. P.; Jen, A. *Nat. Biotechnol.* **2002**, *20*, 789−790.
(13) Shenoy, B.; Wang, Y.; Shan, W.; Margolin, A. L. *Biotechnol. Bioeng.* **2001**, *73*, 358−369.
(14) Yang, M. X.; Shenoy, B.; Disttler, M.; Patel, R.; McGrath, M.; Pechenov, S.; Margolin, A. L. *Proc. Natl. Acad. Sci. U. S. A.* **2003**, *100*, 6934−6939.
(15) Judge, R. A.; Forsythe, E. L.; Pusey, M. L. *Biotechnol. Bioeng.* **1998**, *59*, 776−785.
(16) Dos Santos, R.; Carvalho, A. L.; Roque, A. C. A. *Biotechnol. Adv.* **2017**, *35*, 41−50.
(17) Clogston, L. C.; Christian, R. T.; Osslund, D. T.; Freeman, E. Sclerostin Antibody Crystals and Formulations Therof. US9145457B2, 2016.
(18) Fraunhofer, W.; Borhani, W. D.; Winter, G.; Gottschalk, S. Compositions and Methods for Crystallizing Antibodies. US8753839B2, 2014.
(19) Norrman, M.; Hubálek, F.; Schluckebier, G. *Eur. J. Pharm. Sci.* **2007**, *30*, 414−423.
(20) Brange, J.; Vølund, A. *Adv. Drug Delivery Rev.* **1999**, *35*, 307−335.
(21) Markussen, J.; Hougaard, P.; Ribel, U.; Sørensen, A. R.; Sørensen, E. *Protein Eng., Des. Sel.* **1987**, *1*, 205−213.
(22) Sultan, M. H.; Mahdi, W. A.; Kwon, Y. M. *Processes* **2020**, *8*, 1320.
(23) Pechenov, S.; Shenoy, B.; Yang, M. X.; Basu, S. K.; Margolin, A. L. *J. Control. Release* **2004**, *96*, 149−158.
(24) Schellekens, H. *NDT Plus* **2009**, *2*, i27−i36.
(25) Mohammad, M. A.; Grimsey, I. M.; Forbes, R. T. *J. Pharm. Biomed. Anal.* **2015**, *114*, 176−183.
(26) Sage, J. T.; Zhang, Y.; McGeehan, J.; Ravelli, R. B. G.; Weik, M.; Van Thor, J. J. *Biochim. Biophys. Acta* **2011**, *1814*, 760−777.
(27) Whitmore, L.; Wallace, B. A. *Biopolym. Orig. Res. Biomol.* **2008**, *89*, 392−400.
(28) Narang, D.; Lento, C.; Wilson, J. D. *Biomedicines* **2020**, *8*, 224.
(29) Maveyraud, L.; Mourey, L. *Molecules* **2020**, *25*, 1030.
(30) Billeter, M.; Wagner, G.; Wüthrich, K. *J. Biomol. NMR* **2008**, *42*, 155−158.
(31) Zhao, X. Protein Structure Determination by Solid-State NMR. In *NMR Proteins and Small Biomolecules*; Springer: Berlin, Heidelberg, 2011; pp. 187−213.
(32) Yip, K. M.; Fischer, N.; Paknia, E.; Chari, A.; Stark, H. *Nature* **2020**, *587*, 157−161.
(33) Berkowitz, S. A.; Engen, J. R.; Mazzeo, J. R.; Jones, G. B. *Nat. Rev. Drug Discov.* **2012**, *11*, 527−540.
(34) Alsenaidy, M. A.; Jain, N. K.; Kim, J. H.; Middaugh, C. R.; Volkin, D. B. *Front. Pharmacol.* **2014**, *5*, 39.
(35) Sörgel, F.; Lerch, H.; Lauber, T. *BioDrugs* **2010**, *24*, 347−357.
(36) Metz, G.; Wu, X. L.; Smith, S. O. *J. Magn. Reson. Ser. A* **1994**, *110*, 219−227.
(37) Weingarth, M.; Tekely, P.; Bodenhausen, G. *Chem. Phys. Lett.* **2008**, *466*, 247−251.
(38) Wang, D.; Park, J.; Patil, S. M.; Smith, C. J.; Leazer, J. L., Jr.; Keire, D. A.; Chen, K. *J. Pharm. Sci.* **2020**, *109*, 1519−1528.
(39) Bramham, J. E.; Podmore, A.; Davies, S. A.; Golovanov, A. P. *ACS Pharmacol. Transl. Sci.* **2021**, *4*, 288−295.
(40) Li, M.; Reichert, P.; Narasimhan, C.; Sorman, B.; Xu, W.; Cote, A.; Su, Y. *Mol. Pharmaceutics* **2022**, *19*, 936−952.
(41) Andrew, E. R.; Eades, R. G. *Proc. R. Soc. London. Ser. A. Math. Phys. Sci.* **1953**, *216*, 398−412.
(42) KovaL'Akova, M.; Fričová, O.; Hutníková, M.; Hronský, V.; Olčák, D. *Acta Phys. Pol. A* **2017**, *131*, 1162−1164.
(43) Fyfe, C. A.; Lewis, A. R.; Chézeau, J.-M. *Can. J. Chem.* **1999**, *77*, 1984−1993.
(44) Müller, L.; Kumar, A.; Baumann, T.; Ernst, R. R. *Phys. Rev. Lett.* **1974**, *32*, 1402.
(45) Ramamoorthy, A.; Wei, Y.; Lee, D.-K. *Annu. Rep. NMR Spectrosc.* **2004**, *52*, 1−52.
(46) Huster, D.; Schiller, J.; Arnold, K. *Magn. Reson. Med.* **2002**, *48*, 624−632.
(47) Knight, M. J.; Webber, A. L.; Pell, A. J.; Guerry, P.; Barbet-Massin, E.; Bertini, I.; Felli, I. C.; Gonnelli, L.; Pierattelli, R.; Emsley, L.; Lesage, A.; Herrmann, T.; Pintacuda, G. *Angew. Chem. Int. Ed.* **2011**, *123*, 11901−11905.
(48) Zhou, D. H.; Rienstra, C. M. *J. Magn. Reson.* **2008**, *192*, 167−172.
(49) Balschmidt, P. *ASPB28 Insulin Crystals*. Google Patents, November 24, 2008.
(50) Norrman, M.; Ståhl, K.; Schluckebier, G.; Al-Karadaghi, S. *J. Appl. Crystallogr.* **2006**, *39*, 391−400.

(51) Bishnoi, A.; Kumar, S.; Joshi, N. Wide-Angle X-Ray Diffraction (WXRD): Technique for Characterization of Nanomaterials and Polymer Nanocomposites. In *Microscopy Methods in Nanomaterials Characterization*; Elsevier, 2017; pp. 313−337.

https://doi.org/10.1021/acs.analchem.2c05485
Anal. Chem. 2023, 95, 8469−8477

pubs.acs.org/ac

analytical chemistry

CELEBRATING 95 YEARS

June 6, 2023 Volume 95 Number 22

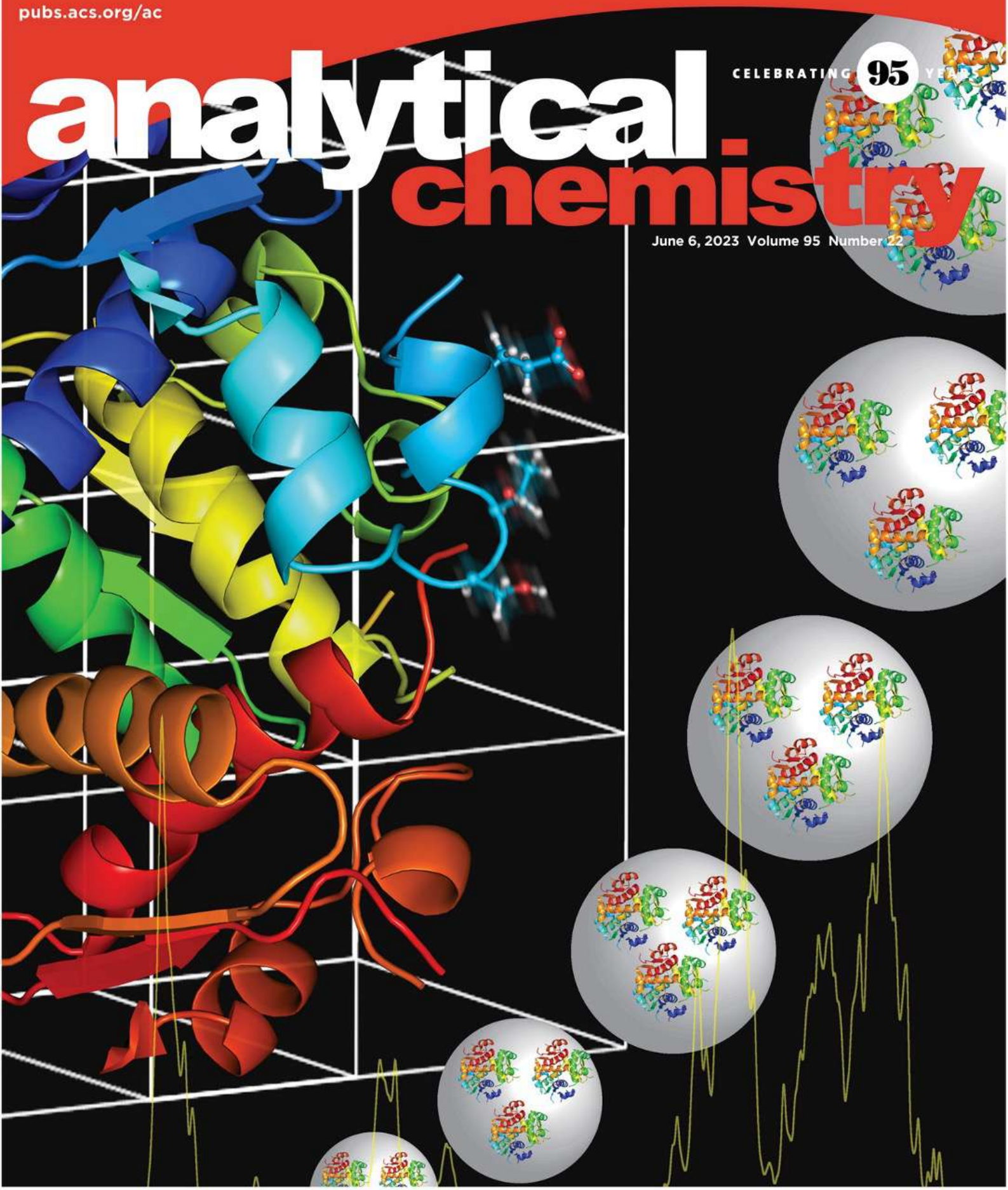

ACS Publications
Most Trusted. Most Cited. Most Read.

www.acs.org

analytical chemistry

pubs.acs.org/ac Article

Exploring the Higher Order Structure and Conformational Transitions in Insulin Microcrystalline Biopharmaceuticals by Proton-Detected Solid-State Nuclear Magnetic Resonance at Natural Abundance

Soumya Ranjan Pujahari,[#] Rudra N. Purusottam,[#] Pramod S. Mali, Sambeda Sarkar, Navin Khaneja, Navratna Vajpai,* and Ashutosh Kumar*

Cite This: *Anal. Chem.* 2024, 96, 4756−4763 Read Online

ACCESS | Metrics & More | Article Recommendations | Supporting Information

ABSTRACT: The integrity of a higher order structure (HOS) is an essential requirement to ensure the efficacy, stability, and safety of protein therapeutics. Solution-state nuclear magnetic resonance (NMR) occupies a unique niche as one of the most promising methods to access atomic-level structural information on soluble biopharmaceutical formulations. Another major class of drugs is poorly soluble, such as microcrystalline suspensions, which poses significant challenges for the characterization of the active ingredient in its native state. Here, we have demonstrated a solid-state NMR method for HOS characterization of biopharmaceutical suspensions employing a selective excitation scheme under fast magic angle spinning (MAS). The applicability of the method is shown on commercial insulin suspensions at natural isotopic abundance. Selective excitation aided with proton detection and non-uniform sampling (NUS) provides improved sensitivity and resolution. The enhanced resolution enabled us to demonstrate the first experimental evidence of a phenol-escaping pathway in insulin, leading to conformational transitions to different hexameric states. This approach has the potential to serve as a valuable means for meticulously examining microcrystalline biopharmaceutical suspensions, which was previously not attainable in their native formulation states and can be seamlessly extended to other classes of biopharmaceuticals such as mAbs and other microcrystalline proteins.

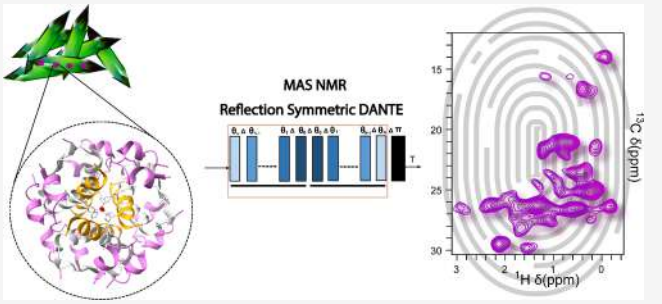

A higher order structure (HOS) is an essential requirement for understanding the molecular structure and defining the critical quality attributes (CQAs) of protein therapeutics.[1] Altered HOS can significantly impact the stability, quality, safety, and efficacy of these products, increasing the risk of immunogenicity and the loss of function. Therefore, the characterization of biotherapeutics in their native formulated state is crucial. Several biophysical techniques are routinely used for biopharmaceutical characterization, such as fluorescence spectroscopy,[2] differential scanning calorimetry (DSC),[3] H/D exchange mass spectrometry (HDX-MS),[4] Fourier transform infrared spectroscopy (FT-IR),[5] X-ray diffraction,[3,6] circular dichroism (CD),[7] nuclear magnetic resonance (NMR),[8−15] and cryo-electron microscopy (cryo-EM).[16] Most of the biophysical techniques require treatment of the samples, such as additional efforts for sample concentration or special treatments during sample preparation (such as acidification) or buffer exchange. In contrast, NMR offers several advantages compared to other techniques, including high resolution and requiring no or minimum sample treatment. Consequently, NMR is particularly well suited for characterizing biopharmaceuticals in situations in which manipulation of the formulated samples is not needed.

Based on their physical properties, parenteral formulations for biotherapeutics can be categorized into solution-ready formulation, lyophilized powder or freeze-dried (ready to be mixed with the solvent), crystalline suspension, and biphasic suspension (where solid state and liquid state coexist). When dealing with highly concentrated protein drugs or the need for controlled drug release, microcrystalline/biphasic drugs are favored due to their lower likelihood of aggregation, phase separation, self-association, and viscosity compared to solution formulations.[17] The use of drugs in microcrystalline suspension form enhances their bioavailability and allows for sustained release compared to other dosage forms.[18−20] Although insulin

Received: September 8, 2023
Revised: January 31, 2024
Accepted: January 31, 2024
Published: February 8, 2024

remains the only licensed microcrystalline suspension drug available in the market for patient usage, biopharmaceutical industries have recently focused on developing full-length monoclonal antibodies (mAbs) suitable for batch-scale production and human administration using crystallization techniques.[21,22] The HOS of insulin has been studied in detail both in solution[23] and suspension[24,25] formulations, and it was concluded that insulin exists in a hexameric form stabilized by two zinc (Zn^{2+}) ions and a phenolic compound (i.e., *m*-cresol)[24] present in the microcrystals. Upon injection at the subcutaneous site, while the solution insulin quickly goes into the bloodstream, the microcrystals of the suspension formulation form a concentrated heap at the site of injection.[26,27] The microcrystalline heap, upon dissolution, releases soluble insulin as hexamers, which in turn dissociates into dimers and monomers, each with a different dissociation constant, facilitating controlled release.[28] As the formulation of the drug product was carried out in its microcrystalline state, the investigation of the HOS of the protein (drug) in the native state (crystalline form) is of utmost importance.

Solid-state nuclear magnetic resonance (ssNMR) spectroscopy plays an essential role in the field of small molecule pharmaceutical analysis, as nearly 80% of formulated drug products are available in different solid forms. ssNMR provides valuable atomic-level information throughout the drug development process. However, the commonly used ^{13}C detection methods for studying pharmaceutical products face challenges due to the low natural abundance of this isotope, resulting in less sensitive experiments and longer acquisition times. Lately, with the development of ultrafast magic-angle spinning (MAS) NMR probes, it is now possible to incorporate ^{1}H detection schemes in solid-state NMR.[29] This significantly benefits from its rich abundance and high gyromagnetic ratio to obtain the sensitivity enhancement necessary for natural abundance samples. These advances allowed the extension of the ssNMR application to suspension formulations of therapeutic proteins.[30] In pharmaceutical characterization, many established 2D methods employing proton detection primarily focus on $^{1}H-^{1}H$, $^{15}N-^{1}H$, and $^{13}C-^{1}H$ correlation spectra, serving as distinctive patterns for identifying and analyzing pharmaceutical substances.[30,31] It is worth mentioning that proton-detected solid-state NMR (ssNMR) is also used for determining the structure of amyloid fibrils; however, the samples tend to have broadened linewidths due to their inherent inhomogeneity.[32] Nevertheless, there are notable studies in this area; Daskalov et al.[33] demonstrated the high-resolution structure of HELLF fibrils, while Bahri et al.[34] revealed both close-contact and long-distance interactions within Ab (1−42) fibrils exclusively through proton detection. Shi et al.[35] investigated the helical structure of the cytoskeletal bactofilin BacA where proton detection was used. However, it should be noted that these samples were isotopically labeled for resonance assignment and $^{1}H-^{1}H$ distances were used for structure calculations.

The side chains of amino acids play a crucial role in maintaining the three-dimensional structure of proteins and the arrangement of subunits in protein complexes. Since the folding and shape of the protein directly impact the functionality of a protein drug, side chains can provide valuable insights into the structural integrity. The latest guidelines for developing biosimilars strongly recommend reporting on the folding and aggregation properties, as well as characterizing higher order structures (HOSs). Methyl groups, in particular, have been extensively used in biomolecular NMR as highly sensitive site-specific probes for structure,[36−39] dynamics,[40,41] and interaction studies.[42−44] Due to their well-dispersed nature in the protein's 3D structure, methyl chemical shifts can provide valuable information on subtle alterations inside the hydrophobic pocket of the protein that can alter the native folding as well as potential changes in the oligomerization state of a protein. Alternatively, these can also be explored for identifying binding epitopes in the protein−receptor interactions.[45] In a previous study involving microcrystalline suspension, we demonstrated the comparability of higher order structures through the use of a 1D ^{13}C CP-MAS technique, followed by principal component analysis and the calculation of Mahalanobis distance.[25] We also attempted to compare the spectral data of the ^{1}H-detected $^{13}C-^{1}H$ HETCOR experiment; however, we encountered limitations in achieving sufficient resolution.

This study introduces a novel approach for solid-state NMR analysis of biopharmaceutical suspensions at fast magic-angle spinning (MAS), specifically targeting the methyl and aliphatic side-chain characteristics. The proposed method incorporates a unique band selective excitation scheme and combines proton detection with non-uniform sampling (NUS) to reduce the time required for spectrum acquisition. The reconstruction of NUS data using a compressed sensing algorithm further enhances the resolution, allowing for site-specific characterization of the higher order structure of insulin in its microcrystalline suspensions. Recent applications of solid-state NMR in studying amorphous drugs have shown promising results by combining machine-learning tools, such as ShiftML, for chemical shift predictions to aid in the assignment of one- and two-dimensional NMR spectra.[46,47] In our study, we also utilized a similar machine-learning platform called SHIFTX2, which combines ensemble machine-learning methods with sequence alignment-based approaches to calculate protein chemical shifts for both backbone and side-chain atoms.[48] The predicted chemical shifts were instrumental in the assignment of a few key resonances in the 2D $^{13}C-^{1}H$ HETCOR spectra. Insulin, in its drug-formulated state, exists in a thermodynamically stable hexameric state, exhibiting conformational dynamics between R6, T6, and T3R3 states. With substantially enhanced resolution and SHIFTX2-predicted assignments, we were able to deduce the diverse range of conformational populations and elucidate the potential mechanism of interconversion between these conformational states.

EXPERIMENTAL SECTION

Sample Preparation. Uniformly ^{13}C, ^{15}N-labeled microcrystalline SH3 domain protein was purchased from Cambridge Isotope Laboratories, Inc. Humulin 70/30 (mixture of regular human insulin, Humulin R, and the intermediate action of Humulin N isophane suspension) and Humulin N (isophane insulin human suspension) by Eli Lilly were purchased from over the counter. Two milliliters of the insulin suspension was centrifuged at 500*g* for 15−20 min. The loose pellet was then transferred to 1.9 mm ZrO_2 rotors. The Vespel rotor caps were sealed with epoxy glue to maintain the hydration level of the samples.

NMR Spectroscopy. All solid-state NMR experiments were performed on a Bruker Avance III spectrometer operating at a ^{1}H Larmor frequency of 750 MHz and MAS frequency of 33 kHz by using a Bruker 1.9 mm H/C/N CP MAS triple

https://doi.org/10.1021/acs.analchem.3c04040
Anal. Chem. 2024, 96, 4756−4763

resonance probe. The first (^{1}H−^{13}C) and second (^{13}C−^{1}H) cross-polarization (CP) contact times were 1.2 and 0.3−0.4 ms, respectively. The MISSISSIPPI[49] scheme of 100−200 ms was used for solvent suppression. The PISSARRO[50] scheme was used for efficient heteronuclear decoupling in the spinning regime used in the study.[45,51] Experiments were conducted at 298 K, and the temperature was calibrated by the chemical shift of DSS (4,4-dimethyl-4-silapentane-1-sulfonic acid). NUS 2D spectra were acquired by using 25% sampling corresponding to 64 t1 points in the indirect dimension and a recycling delay of 1.5 s. We opted for sinusoidal weighted Poisson gap sampling, which is generally accepted as the most robust of all and has high-fidelity postreconstruction. The recommended NUS of 25% for two-dimensional experiments after reconstitution produces results similar to those from uniform sampling. The sampling schedule was generated using the HMSist "nusPGSv3" AU macro in TopSpin (Version 3.6). Acquired NUS data was processed by hmsIST (Iterative Soft Threshold) inside TopSpin. For the band-selective excitation, a total of two DANTE blocks were used, each containing six pulses separated by a rotor period. The second block is the reverse/mirror symmetry of the earlier. The first six rotor periods are 0.0307, 0.0345, 0.0375, 0.0398, 0.0412, and 0.0208 multiples of ^{13}C 180° pulse followed by a final delay of 0.1579 ms.

Chemical Shift Predictions. The assignment of 2D ^{13}C−^{1}H HETCOR spectra was done from predicted chemical shifts of insulin hexamers using SHIFTX2 program version 1.10 (http://www.shiftx2.ca/index.html). PDB IDs: 1ZNJ (R6) and 1MSO (T6). A pH value of 7 and a temperature of 298 K were used for the predictions.

RESULTS AND DISCUSSION

Band Selective Excitation Pulse Design. Selective excitation of a particular nuclei or bandwidth has played a crucial role in the development of advanced pulse sequences for spectral manipulation in solution and solid-state NMR. In the realm of solids, selective excitation finds extensive applications in multidimensional spectrum assignment, distance measurements, and overcoming spectral overlap in uniformly labeled systems. Existing approaches for achieving selective excitation include the use of Gaussian-shaped pulses,[52] DANTE (delay alternating with nutation for tailored excitation[53,54]), heteronuclear selective phase-optimized recoupling (hetSPR),[55] SELDOM (SELectivity by Destruction Of Magnetization),[56] or computer-optimized E-family sequences.[57] In this study, we introduce a reflection symmetric version of the DANTE sequence with variable flip angles, followed by a hard π pulse and a specific delay time for band selective excitation (Figure 1 and Figure S1). This allowed the selection of desirable aliphatic side-chain resonances in the ^{13}C−^{1}H HETCOR spectra with enhanced resolution. A comprehensive theoretical formulation of this sequence is provided in the Supporting Information.

Testing the Performance of Selective Excitation on Microcrystalline SH3 Protein. To showcase the effectiveness of the selective excitation scheme, we conducted an initial test on a microcrystalline protein called the alpha-SH3 domain, which was uniformly labeled with ^{13}C and ^{15}N isotopes. The two reflection symmetric excitation blocks of DANTE were integrated into the ^{13}C channel of a 2D HETCOR experiment, with proton detection, as outlined in the pulse program

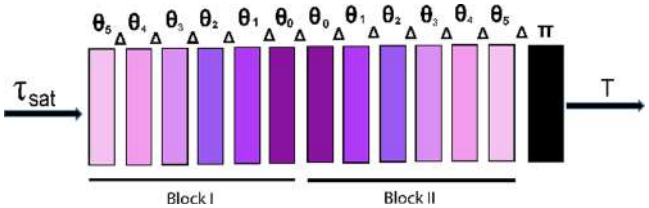

Figure 1. The figure shows the scheme of reflection symmetric DANTE (where Δ (delay) = 26.31 μs, θ_0 = π*0.0208, θ_1 = π*0.0412, θ_2 = π*0.0398, θ_3 = π*0.0375, θ_4 = π*0.0345, θ_5 = π*0.0307, and π = 180° hard pulse in the carbon channel).

(Figure 2a). By employing the reflection symmetric DANTE sequence on the ^{13}C nuclei, we were able to selectively excite

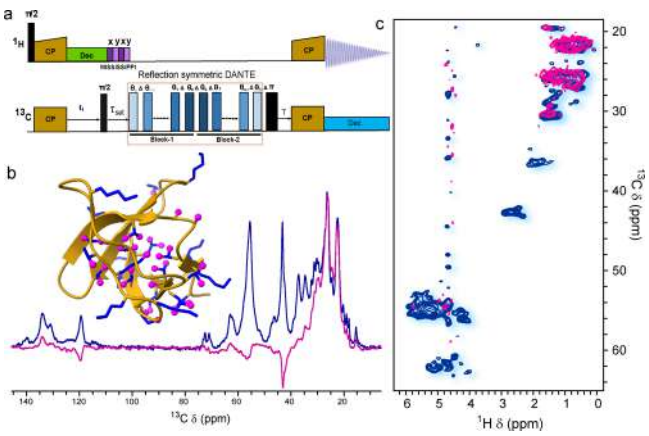

Figure 2. (a) Pulse diagram to acquire methyl and aliphatic side-chain fingerprint employing ^{1}H detection. (b) One-dimensional ^{13}C spectra of the microcrystalline SH3 domain showing the performance of selective excitation scheme (pink) and broadband excitation (blue). (c) Overlay spectra of 2D ^{13}C−^{1}H CP-HETCOR without a reflection symmetric DANTE block incorporated with ^{1}H detection (blue) and by using the novel pulse scheme shown in Figure 2a (pink).

the narrow ^{13}C region encompassing methyl, methine, and methylene side-chain resonances (0 to ∼30 ppm) while effectively suppressing unwanted signals from other regions, as depicted in Figure 2b. For comparison, the one-dimensional ^{13}C spectra of the aliphatic region were obtained using 90° hard pulse broadband excitation. Additionally, we conducted a 2D ^{1}H-detected ^{13}C−^{1}H HETCOR version of the selective excitation experiment, and the corresponding results are presented in Figure 2c. The spectral profile of the newly designed pulse scheme shows a near-perfect overlap with the traditional 2D ^{13}C−^{1}H HETCOR experiment in the methyl and methylene region (0 to ∼30 ppm). However, no significant enhancement in the resolution could be obtained. At a high field (750 MHz) and high abundance of isotopically labeled ^{13}C, strong dipolar coupling-induced anisotropic effects are likely to have contributed to line broadening and poor resolution. Also, the inherent heterogeneous nature of the sample cannot be ruled out. This inclined us to test our hypothesis on suspension formulations of human insulin, which is present in its natural abundant state and is well studied to exist in a microcrystalline state, with crystal size varying between 3 and 8 μm.[25] These crystals are well studied by X-ray crystallography and reported to have a single hexameric unit per crystal and remaining solvent.[24]

https://doi.org/10.1021/acs.analchem.3c04040
Anal. Chem. 2024, 96, 4756−4763

Resolution Enhancement in Insulin Suspensions at Natural Abundance. In the previous study conducted by Zhou et al., the viability of proton-detected 2D $^{13}C-^{1}H$ and $^{15}N-^{1}H$ CP-HETCOR techniques on biopharmaceuticals at their natural isotopic abundance was demonstrated.[30] This study focused on the backbone (−CH) region of the $^{13}C-^{1}H$ HETCOR spectrum, providing valuable information regarding the overall folding pattern of protein-based pharmaceuticals. In the current study, our focus was primarily on the sensitivity and resolution enhancement in the methyl and aliphatic side-chain regions of the spectrum, which offer insights into the secondary, tertiary, and quaternary structural features collectively termed as the higher order structure (HOS).

Proton-detected 2D $^{13}C-^{1}H$ HETCOR experiment at carbon-13 natural abundance can sometimes take a significant amount of time to achieve a decent signal-to-noise (S/N) ratio compared to uniformly labeled protein samples. To significantly reduce on acquisition time, we incorporated non-uniform sampling (NUS), which is quite common in recording multidimensional spectra in biomolecular NMR.[58−60] However, it is not widely used in pharmaceutical solid-state NMR applications, where the low natural abundance of NMR active isotopes is usually a limiting factor. Over the years, several NUS schemes have been proposed to sample time domain signals more frequently when the signal is strong and less when it is weak.[61,62] There are only a few studies employing solid-state NMR where a detailed analysis of NUS schemes has been described.[63−65] Conventional data processing methods such as fast Fourier transformation (FFT) and linear prediction (LP) cannot be applied to data collected by NUS. Instead, different algorithms, including maximum entropy, maximum likelihood method (MLM), multidimensional decomposition (MDD), and compressed sensing (CS), are used for the reconstruction of NUS data. For the current study, we opted for the sinusoidal Poisson-gap sampling scheme for acquisition and compressed sensing for reconstruction and processing that has been shown to enhance the resolution of the spectra with high fidelity.[66−68]

We performed ^{1}H-detected 2D $^{13}C-^{1}H$ HETCOR experiments on representative batches of Humulin N (100% suspension) and Humulin 70/30 (biphasic mix of 70 parts of suspension human insulin and 30 parts of soluble human insulin) and observed a significant spectral overlap between both (Figure 3a), indicating comparable HOS of human insulin in the two drug products despite minor differences in the formulations. Subsequently, we repeated the experiment with the reflection symmetry DANTE incorporated in ^{1}H-detected 2D $^{13}C-^{1}H$ HETCOR on both samples (Figure 3d,e), where we have selectively excited the methyl and aliphatic regions (0−30 ppm). By adjusting the magnetization transfer scheme in the heteronuclear correlation (HETCOR) experiment and reconstruction of NUS data by a compressed sensing algorithm, it is possible to obtain information from either the mobile or rigid components.[69] The spectral profile, thus obtained, in the selected region showed improvement in resolution and an increase in S/N of about ∼2−2.5-fold (Figure S3), which is noticeable from the appearance of flexible methyl peaks (below 20 ppm). The observed linewidth of Humulin N decreased from 305 to 188 Hz (∼40% reduction) and, for Humulin 70/30, it decreased from 182 to 149 Hz (∼20% reduction) (Figure S2). The enhanced resolution and sensitivity allowed us to investigate the higher order structure of insulin in the microcrystalline suspension without perturbing the crystalline state of samples and preserving the overall higher order structure.

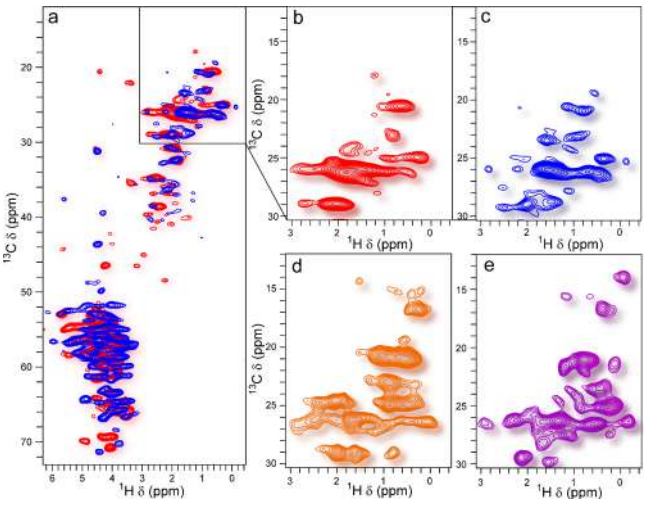

Figure 3. (a) 2D $^{13}C-^{1}H$ CP-HETCOR overlay of Humulin N (red) and Humulin 70/30 (blue) with ^{1}H detection. (b, c) Zoomed region from the overlay spectra of panel (a). (d, e) 2D $^{13}C-^{1}H$ CP-HETCOR with ^{1}H detection using the pulse sequence shown in panel (a) (with the reflection symmetric DANTE block) of Humulin N (orange) and Humulin 70/30 (magenta), respectively.

Allosteric Transition of Hexameric Insulin. The intrinsic property of insulin is to self-associate, which plays a key role in therapeutic formulations. In particular, the hexameric state is promoted by the presence of phenolic ligands and Zn^{2+} (or other divalent transition metals) that exhibit greater stability than insulin dimers and monomers and hence are needed for a longer shelf life.[70] Metal-bound insulin hexamers also exhibit phenol-induced allostery.[71−73] Insulin can coexist in equilibrium as a mixture of all taut (T_6), all relaxed (R_6), or half taut−half relaxed (T_3R_3) protein conformations[74−77] (Figure 4a). The structural difference between the T-state and the R-state is only in the first 8 amino acids of the B-chain of the insulin monomer, where B1−B8 fold into a helical state in the R-state in the presence of phenolic ligands, while they remain in an extended conformation in the T-state. The T−R transition has been reported by using different biophysical techniques such as circular dichroism (CD),[78] FTIR,[79] and Raman spectroscopy,[80] and the representative crystal states are available in the literature.[81−83] Although the physiological significance of the T- and R-states is unknown, it has been proposed that the R-state is primarily associated with the higher stability of insulin in its formulated state. The T-state is crucial for correct proinsulin and/or insulin folding[73,84] and is biologically more relevant. However, due to limited structural information, insulin receptor binding does not always entail the T- or R-state.[85,86] The two hexameric states, T_6 and R_6, differ significantly in their dissociation kinetics, with the T_6 state prevailing in the physiological settings and undergoing dissociation to dimers within a few minutes, while the R_6 state has a significantly longer lifetime ranging from hours to days.[87,88] To increase the shelf life of therapeutic formulations, phenol is often added as an excipient as it tilts the equilibrium toward the more long-lasting R_6 state.[89] This is expected to decrease dissociation and subsequently prevent the occurrence of off-pathway equilibria. The existence of multiple hexameric states observed in solution as well as in amorphous and

https://doi.org/10.1021/acs.analchem.3c04040
Anal. Chem. 2024, 96, 4756−4763

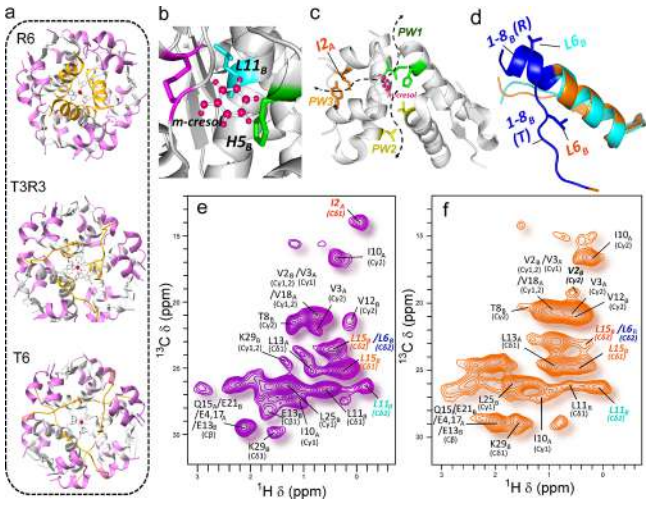

Figure 4. (a) Different hexameric conformations of insulin: insulin R6 (PDB: 1ZNJ), insulin T3R3 (1TRZ), and insulin T6 (1MSO). (b) Hydrophobic pocket of the R form of insulin involving CysA6 and CysA11 (both marked in purple), HisB5 (green), and Leu11 of B-chain (cyan). (c) Different phenol escape pathways named PW1, PW2, and PW3 and respective gatekeeper residues marked as IleA10, HisB5 (PW1: green), LeuA13, LeuB17 (PW2: yellow), IleA2, and TyrA19 (PW3: orange). (d) Superimposed B-chain of insulin R form (cyan) and T form (orange); first 1−8 amino acids of both forms marked in blue. (e) Most probable resonance assignment of 2D ^{13}C−^{1}H HETCOR with the reflection symmetric DANTE block of Humulin 70/30 (chemical shift predicted from SHIFTX2). (f) Most probable resonance assignment of 2D ^{13}C−^{1}H HETCOR with the reflection symmetric DANTE block of Humulin N (chemical shift predicted from SHIFTX2).

crystalline states is a clear link to the occurrence of phenol-bound allostery.[79,90,91]

With the improved sensitivity and resolution of methyl peaks, we were able to discern mechanistic snapshots from the representative spectra of Humulin N and Humulin 70/30. Structural features were deduced from the chemical shift predictions for the insulin hexamer with the help of an online server called SHIFTX2[48] (Table S1). The predicted and experimental spectra showed very good correlation, which allowed putative assignment of a few important peaks, representative of different conformational states of human insulin. An upfield-shifted peak in the ω_1-dimension (^{1}H: −0.175 ppm) was observed in selective methyl spectra of Humulin 70/30 (Figure 4e, labeled in cyan). The phenolic ligand in the R_6 hexamer largely resides in a hydrophobic pocket at the dimer−dimer interface, which is formed by HisB5, LeuB11, and residues CysA6 and CysA11[89] (Figure 4b) from different dimer subunits. As the methyl of residue LeuB11 is surrounded by highly hydrophobic groups, the corresponding resonance is expected to show an upfield shift. The peak below 0 ppm was therefore assigned as LeuB11, and it is also labeled as a marker for insulin in a predominantly R_6 hexamer conformation, as in a T_6 or T_3R_3 state, the dimer interface would be less crowded, and therefore, an upfield shift is not expected. Interestingly, this peak was found missing and/or shifted downfield in the Humulin N spectrum (Figure 4f), indicative of an alternative hexameric state(s) (T_6 or T_3R_3). In the T-state, the enhanced flexibility of the B1−B8 residues (Figure 4d) would lead to a decrease in the magnetization transfer via dipolar couplings, which will be reflected as a decrease in the intensity of the corresponding peaks in the B1−B8 residues. This was well corroborated as the decreased intensity of the LeuB6 peak in the Humulin N spectrum, indicating LeuB6 to be another marker peak for the identification of enhanced T-state contributions in the hexamer. Further, a weighted average combination of different ratios of PDB structures in the absence (T6 conformation; PDB ID: 1MSO) and presence (R6 conformation; PDB ID: 1ZNJ) of a phenolic ligand was used for back prediction of chemical shifts. A comparatively better match with 95% of R6:1ZNJ and 5% of T6:1MSO was observed for Humulin 70/30, and that with 75% of R6:1ZNJ and 25% of T6:1MSO was observed for Humulin N (Figure S4).

To the best of our knowledge, this is the first NMR study that could demonstrate evidence of different hexameric states in the insulin suspensions using methyl peak markers. The conformational fluctuations among different hexameric states are a well-known phenomenon as is also demonstrated by single crystal X-ray studies, where each of the three states could be crystallized.[81−83] These conformational fluctuations happen due to the dynamic movement of the phenolic ligands ("in" and "out" from the hexamer) present in the drug formulations. These "in" and "out" movements have been studied as "ligand escaping pathways" using computational biology tools, primarily using molecular dynamic simulations.[87,92]

The studies by Vashisth et al.[92] and Adam et al.[87] revealed the existence of three distinct escaping pathways (named PW1, PW2, and PW3) of phenol from its hydrophobic core (Figure 4c). In PW1, the process of phenol escape is accomplished via a gate-pushing mechanism, wherein the phenol molecule forces its way through the "gatekeeper" residues IleA10 and HisF5. On the other hand, PW2 involves a gate-hopping mechanism whereby the phenol molecule utilizes an existing escape channel located between IleA10/HisF5 and LeuA13/LeuH17 (insulin hexameric subunits are named from A−F). PW3 follows a different pathway, as the phenol molecule escapes through a densely packed region in the insulin monomer's core, primarily comprised of chains A and B, and is predominantly lined by specific residues such as IleA2, Gln A5, CysA6, CysA11, LeuA16, TyrA19, LeuB11, and LeuB15. The two residues IleA2 and TyrA19 act as gatekeeper residues for PW3.[87] Through MD simulations, Antoszewski et al. have also shown an increase in solvation of the phenol and gatekeeper residues during phenol escape from its hydrophobic core.[87] This increase in the hydration level of IleA2 (gatekeeper residue of PW3) will potentially lead to an increase in the flexibility of IleA2 side chains. Interestingly, the intensity of the IleA2 peak is minimal, as observed in Humulin N, indicative of the release of the phenolic ligand via the PW3 pathway. This is further corroborated by observing the change in the intensity of LeuB15 in Humulin N in comparison to Humulin 70/30 spectra. In total, the enhanced resolution in the indirect dimension has provided sufficient information to deduce multiple transitions involved in the insulin hexameric states. It is to be noted that slightly different conformations observed in the two insulin suspension formulations represent the dynamic picture of the insulin hexameric states due to rearrangements of phenolic ligands. While these differences may have some impact on product stability, these differences are not expected to have any meaningful clinical differences, as the biologically active moiety in insulin is its monomer. Nonetheless, our novel experimental scheme allowed for discerning different states of insulin, and we believe that it

https://doi.org/10.1021/acs.analchem.3c04040
Anal. Chem. 2024, 96, 4756−4763

can be extended to other biopharmaceuticals, where different states may lead to safety or immunogenicity concerns. The proton-detection MAS with a NUS sampling scheme proposed in this work offers a high-resolution structural approach to comprehensively differentiating various conformations between two formulations of biopharmaceuticals. The signature obtained in a residue type or at the chemical moiety level exceeds the capabilities of other analytical methods such as powder X-ray diffraction or SAXS typically used for microcrystalline or amorphous samples. The diffraction patterns obtained from these techniques for large microcrystalline protein/mAb therapeutics generate limited structural information. Therefore, we believe that the proposed method can serve as an advanced tool in drug development, investigating protein instability events, and quality control.

CONCLUSIONS

In this study, we introduced a technique for obtaining methyl and aliphatic side-chain spectral fingerprints with the site-specific resolution of pharmaceutical insulin suspensions. The combination of a novel selective excitation scheme, proton detection at fast MAS, and non-uniform sampling provides mechanistic insights into the higher order structure of pharmaceutical insulin. The use of non-uniform sampling improved the signal-to-noise ratio and sensitivity of multiple peaks, achieving a resolution in the indirect dimension that was not achievable with traditional uniform acquisition at natural isotopic abundance. The enhanced resolution and sensitivity allowed us to experimentally observe different hexameric states in insulin formulations. Additionally, the current study identified the ligand (phenol) escape route from the protein complex (insulin hexamer) on the basis of the change in intensities observed for key marker residues. To the best of our knowledge, this is the first detailed experimental evidence of the key residues involved in a phenol escaping pathway leading to conformational transitions to different hexameric states in insulin. This approach can be seamlessly extended to crystalline suspensions of monoclonal antibodies (mAbs), which are being considered as a potential alternative formulation strategy for subcutaneous delivery at high concentrations.[93] As the molecular weight increases, the resolution tends to decrease; nevertheless, our approach allows for a notably improved enhancement in both sensitivity and resolution, and therefore, structural details of complex biopharmaceuticals can be deduced in a precise manner. In summary, the method we presented can be applied to a wide range of protein pharmaceuticals in the suspension state, allowing for the determination of atomic-level higher order structural information previously not attainable in their native formulation state.

ASSOCIATED CONTENT

Supporting Information

The Supporting Information is available free of charge at https://pubs.acs.org/doi/10.1021/acs.analchem.3c04040.

Design of the reflection symmetric DANTE sequence, linewidth comparison of nonselective and selective excitation spectra, predicted chemical shift of the insulin hexamer, and overlay of experimental and predicted ssNMR spectra of insulin (PDF)

AUTHOR INFORMATION

Corresponding Authors

Navratna Vajpai − *Biocon Biologics Limited, Biocon SEZ, Bangalore 560099, India*; Email: navaratna.vajpai@biocon.com

Ashutosh Kumar − *Department of Biosciences and Bioengineering, Indian Institute of Technology, Bombay, Powai Mumbai 400076, India*; orcid.org/0000-0002-5061-8162; Email: ashutoshk@iitb.ac.in

Authors

Soumya Ranjan Pujahari − *Department of Biosciences and Bioengineering, Indian Institute of Technology, Bombay, Powai Mumbai 400076, India*; orcid.org/0000-0002-0739-1732

Rudra N. Purusottam − *Department of Biosciences and Bioengineering, Indian Institute of Technology, Bombay, Powai Mumbai 400076, India*

Pramod S. Mali − *Department of Biosciences and Bioengineering, Indian Institute of Technology, Bombay, Powai Mumbai 400076, India*; orcid.org/0000-0002-8205-2044

Sambeda Sarkar − *System and Control Engineering, Indian Institute of Technology, Bombay, Powai Mumbai 400076, India*

Navin Khaneja − *System and Control Engineering, Indian Institute of Technology, Bombay, Powai Mumbai 400076, India*

Complete contact information is available at: https://pubs.acs.org/10.1021/acs.analchem.3c04040

Author Contributions

#S.R.P. and R.N.P. contributed equally to this work. A.K and N.V. conceived the main idea. S.R.P. and R.N.P. have equal contribution to the work by executing the experimental work and writing the manuscript. S.S. and N.K. carried out the mathematical calculations and design of the pulse sequence. P.S.M. helped in carrying out ssNMR experiments. All authors have given approval to the final version of the manuscript.

Notes

The authors declare no competing financial interest.

ACKNOWLEDGMENTS

This work has been supported by HFNMR 750 MHz, funded by IRCC and IIT Bombay. We acknowledge CSIR for primary financial support. Financial support for this project was also received from IRCC and IIT Bombay.

REFERENCES

(1) Schellekens, H. *NDT Plus* **2009**, *2* (Suppl_1), i27−i36.

(2) Brader, M. L. UV-Absorbance, Fluorescence and FT-IR Spectroscopy in Biopharmaceutical Development. In *Biophys. Charact. Proteins Dev. Biopharm.*; Elsevier, 2020; pp 97−121 DOI: 10.1016/B978-0-444-64173-1.00005-6.

(3) Mohammad, M. A.; Grimsey, I. M.; Forbes, R. T. *J. Pharm. Biomed. Anal.* **2015**, *114*, 176−183.

(4) Narang, D.; Lento, C.; Wilson, J. D. *Biomedicines* **2020**, *8* (7), 224.

(5) Sage, J. T.; Zhang, Y.; McGeehan, J.; Ravelli, R. B. G.; Weik, M.; Van Thor, J. J. *Biochim. Biophys. Acta (BBA)-Proteins Proteomics* **2011**, *1814* (6), 760−777.

(6) Maveyraud, L.; Mourey, L. *Molecules* **2020**, *25* (5), 1030.

(7) Whitmore, L.; Wallace, B. A. *Biopolym. Orig. Res. Biomol.* **2008**, *89* (5), 392−400.
(8) Billeter, M.; Wagner, G.; Wüthrich, K. *J. Biomol. NMR* **2008**, *42* (3), 155−158.
(9) Zhao, X. *NMR Proteins Small Biomol.* **2011**, *326*, 187−213.
(10) Kay, L. E. *J. Magn. Reson.* **2011**, *213* (2), 477−491.
(11) Keller, D.; Clausen, R.; Josefsen, K.; Led, J. J. *Biochemistry* **2001**, *40* (35), 10732−10740.
(12) Olsen, H. B.; Ludvigsen, S.; Kaarsholm, N. C. *Biochemistry* **1996**, *35* (27), 8836−8845.
(13) Kline, A. D.; Justice, R. M., Jr *Biochemistry* **1990**, *29* (12), 2906−2913.
(14) Hua, Q.; Weiss, M. A. *Biochemistry* **1991**, *30* (22), 5505−5515.
(15) Phyo, P.; Zhao, X.; Templeton, A. C.; Xu, W.; Cheung, J. K.; Su, Y. *Adv. Drug Delivery Rev.* **2021**, *174*, 1−29.
(16) Yip, K. M.; Fischer, N.; Paknia, E.; Chari, A.; Stark, H. *Nature* **2020**, *587* (7832), 157−161.
(17) Yang, M. X.; Shenoy, B.; Disttler, M.; Patel, R.; McGrath, M.; Pechenov, S.; Margolin, A. L. *Proc. Natl. Acad. Sci. U. S. A.* **2003**, *100* (12), 6934−6939.
(18) Brange, J.; Vølund, A. *Adv. Drug Delivery Rev.* **1999**, *35* (2−3), 307−335.
(19) Markussen, J.; Hougaard, P.; Ribel, U.; Sørensen, A. R.; Sørensen, E. *Protein Eng. Des. Sel.* **1987**, *1* (3), 205−213.
(20) Sultan, M. H.; Mahdi, W. A.; Kwon, Y. M. *Processes* **2020**, *8* (10), 1320.
(21) Clogston, L. C.; Christian, R. T.; Osslund, D. T.; Freeman, E. Sclerostin Antibody Crystals and Formulations Therof. US20160083460A1 2016.
(22) Fraunhofer, W.; Borhani, W. D.; Winter, G.; Gottschalk, S.Compositions and Methods for Crystallizing Antibodies. US8753839B2 2014
(23) Quinternet, M.; Starck, J.-P.; Delsuc, M.-A.; Kieffer, B. *J. Pharm. Biomed. Anal.* **2013**, *78*−*79*, 252−254.
(24) Norrman, M.; Ståhl, K.; Schluckebier, G.; Al-Karadaghi, S. *J. Appl. Crystallogr.* **2006**, *39* (3), 391−400.
(25) Pujahari, S. R.; Mali, P. S.; Purusottam, R. N.; Kumar, A. *Anal. Chem.* **2023**, *95*, 8469.
(26) Søeborg, T.; Rasmussen, C. H.; Mosekilde, E.; Colding-Jørgensen, M. *Eur. J. Pharm. Sci.* **2009**, *36* (1), 78−90.
(27) Søeborg, T.; Rasmussen, C. H.; Mosekilde, E.; Colding-Jørgensen, M. *Eur. J. Pharm. Sci.* **2012**, *46* (4), 198−208.
(28) Pechenov, S.; Shenoy, B.; Yang, M. X.; Basu, S. K.; Margolin, A. L. *J. Control. release Off. J. Control. Release Soc.* **2004**, *96* (1), 149−158.
(29) Zhou, D. H.; Shah, G.; Cormos, M.; Mullen, C.; Sandoz, D.; Rienstra, C. M. *J. Am. Chem. Soc.* **2007**, *129* (38), 11791−11801.
(30) Zhou, D. H.; Shah, G.; Mullen, C.; Sandoz, D.; Rienstra, C. M. *Angew. Chem.* **2009**, *121* (7), 1279−1282.
(31) Linser, R.; Dasari, M.; Hiller, M.; Higman, V.; Fink, U.; Del Amo, J. L.; Markovic, S.; Handel, L.; Kessler, B.; Schmieder, P.; Oesterhelt, D.; Oschkinat, H.; Reif, B. *Angew. Chem. Int. Ed.* **2011**, *50* (19), 4508−4512.
(32) Liu, J.; Wu, X.-L.; Zeng, Y.-T.; Hu, Z.-H.; Lu, J.-X. *Structure* **2023**, *31*, 230.
(33) Daskalov, A.; Martinez, D.; Coustou, V.; El Mammeri, N.; Berbon, M.; Andreas, L. B.; Bardiaux, B.; Stanek, J.; Noubhani, A.; Kauffmann, B.; Wall, J. S.; Pintacuda, G.; Saupe, S. J.; Habenstein, B.; Loquet, A. *Proc. Natl. Acad. Sci. U. S. A.* **2021**, *118* (1), No. e2014085118.
(34) Bahri, S.; Silvers, R.; Michael, B.; Jaudzems, K.; Lalli, D.; Casano, G.; Ouari, O.; Lesage, A.; Pintacuda, G.; Linse, S.; Griffin, R. G. *Proc. Natl. Acad. Sci. U. S. A.* **2022**, *119* (1), No. e2114413119.
(35) Shi, C.; Fricke, P.; Lin, L.; Chevelkov, V.; Wegstroth, M.; Giller, K.; Becker, S.; Thanbichler, M.; Lange, A. *Sci. Adv.* **2015**, *1* (11), No. e1501087.
(36) Sprangers, R.; Velyvis, A.; Kay, L. E. *Nat. Methods* **2007**, *4* (9), 697−703.
(37) Asami, S.; Reif, B. *Sci. Rep.* **2019**, *9* (1), 1−13.
(38) Majumder, S.; Bhattacharya, D. S.; Langford, A.; Ignatius, A. A. *Pharm. Res.* **2022**, *39* (3), 529−539.
(39) Arbogast, L. W.; Brinson, R. G.; Marino, J. P. *Anal. Chem.* **2015**, *87* (7), 3556−3561.
(40) Rosenzweig, R.; Kay, L. E. *Annu. Rev. Biochem.* **2014**, *83*, 291−315.
(41) Purusottam, R. N.; Tekely, P. *Chem. Phys. Lett.* **2020**, *754*, No. 137628.
(42) Wiesner, S.; Sprangers, R. *Curr. Opin. Struct. Biol.* **2015**, *35*, 60−67.
(43) Zinke, M.; Fricke, P.; Lange, S.; Zinn-Justin, S.; Lange, A. *ChemPhysChem* **2018**, *19* (19), 2457−2460.
(44) Nag, R.; Joshi, S.; Rathore, A. S.; Majumder, S. *J. Am. Chem. Soc.* **2023**, *145*, 10826.
(45) Dey, A.; Mitra, D.; Rachineni, K.; Khatri, L. R.; Paithankar, H.; Vajpai, N.; Kumar, A. *ChemBioChem* **2022**, *23* (23), No. e202200489.
(46) Paruzzo, F. M.; Hofstetter, A.; Musil, F.; De, S.; Ceriotti, M.; Emsley, L. *Nat. Commun.* **2018**, *9* (1), 1−10.
(47) Cordova, M.; Balodis, M.; Hofstetter, A.; Paruzzo, F.; Lill, S. O. N.; Eriksson, E. S. E.; Berruyer, P.; De Almeida, B. S.; Quayle, M. J.; Norberg, S. T.; Ankarberg, A. S.; Schantz, S.; Emsley, L. *Nat. Commun.* **2021**, *12* (1), 1−8.
(48) Han, B.; Liu, Y.; Ginzinger, S. W.; Wishart, D. S. *J. Biomol. NMR* **2011**, *50* (1), 43−57.
(49) Zhou, D. H.; Rienstra, C. M. *J. Magn. Reson.* **2008**, *192* (1), 167−172.
(50) Weingarth, M.; Tekely, P.; Bodenhausen, G. *Chem. Phys. Lett.* **2008**, *466* (4−6), 247−251.
(51) Purusottam, R. N.; Bodenhausen, G.; Tekely, P. *Chem. Phys. Lett.* **2014**, *614*, 220−225.
(52) Bauer, C.; Freeman, R.; Frenkiel, T.; Keeler, J.; Shaka, A. J. *J. Magn. Reson.* **1984**, *58* (3), 442−457.
(53) Caravatti, P.; Bodenhausen, G.; Ernst, R. R. *J. Magn. Reson.* **1983**, *55* (1), 88−103.
(54) Freeman, R. *Chem. Rev.* **1991**, *91* (7), 1397−1412.
(55) Zhang, Z.; Su, Y.; Xiao, H.; Yang, J. *J. Phys. Chem. Lett.* **2022**, *13* (27), 6376−6382.
(56) Tekely, P.; Brondeau, J.; Elbayed, K.; Retournard, A.; Canet, D. *J. Magn. Reson.* **1988**, *80* (3), 509−516.
(57) Veshtort, M.; Griffin, R. G. *ChemPhysChem* **2004**, *5* (6), 834−850.
(58) Billeter, M. *Journal of biomolecular NMR. Springer* **2017**, *68*, 65−66.
(59) Palmer, M. R.; Wenrich, B. R.; Stahlfeld, P.; Rovnyak, D. *J. Biomol. NMR* **2014**, *58* (4), 303−314.
(60) Maciejewski, M. W.; Stern, A. S.; King, G. F.; Hoch, J. C. Nonuniform Sampling in Biomolecular NMR. In *Modern Magnetic Resonance*; Springer, 2008; pp 1305−1311.
(61) Billeter, M.; Orekhov, V. *Novel Sampling Approaches in Higher Dimensional NMR*; Springer Science & Business Media, 2012; Vol. *316*.
(62) Maciejewski, M. W.; Mobli, M.; Schuyler, A. D.; Stern, A. S.; Hoch, J. C. *Nov. Sampl. approaches High. Dimens. NMR* **2011**, *316*, 49−77.
(63) Paramasivam, S.; Suiter, C. L.; Hou, G.; Sun, S.; Palmer, M.; Hoch, J. C.; Rovnyak, D.; Polenova, T. *J. Phys. Chem. B* **2012**, *116* (25), 7416−7427.
(64) Porat, G.; Goldbourt, A. *Isr. J. Chem.* **2019**, *59* (11−12), 1027−1038.
(65) Burakova, E.; Vasa, S. K.; Klein, A.; Linser, R. *J. Biomol. NMR* **2020**, *74* (1), 71−82.
(66) Hyberts, S. G.; Milbradt, A. G.; Wagner, A. B.; Arthanari, H.; Wagner, G. *J. Biomol. NMR* **2012**, *52* (4), 315−327.
(67) Bostock, M.; Nietlispach, D. *Concepts Magn. Reson. Part A* **2017**, *46* (2), No. e21438.
(68) Le Guennec, A.; Dumez, J.; Giraudeau, P.; Caldarelli, S. *Magn. Reson. Chem.* **2015**, *53* (11), 913−920.
(69) Zhang, R.; Nishiyama, Y.; Ramamoorthy, A. *J. Magn. Reson.* **2019**, *309*, No. 106615.

https://doi.org/10.1021/acs.analchem.3c04040
Anal. Chem. 2024, 96, 4756−4763

(70) Norrman, M.; Hubálek, F.; Schluckebier, G. *Eur. J. Pharm. Sci.* **2007**, *30* (5), 414−423.
(71) Roy, M.; Brader, M. L.; Lee, R. W.; Kaarsholm, N. C.; Hansen, J. F.; Dunn, M. F. *J. Biol. Chem.* **1989**, *264* (32), 19081−19085.
(72) Shneine, J.; Voswinkel, M.; Federwisch, M.; Wollmer, A. *Biol. Chem.* **2000**, *381*, 127.
(73) Wan, Z.; Huang, K.; Hu, S.-Q.; Whittaker, J.; Weiss, M. A. *J. Biol. Chem.* **2008**, *283* (30), 21198−21210.
(74) Derewenda, U.; Derewenda, Z.; Dodson, E. J.; Dodson, G. G.; Reynolds, C. D.; Smith, G. D.; Sparks, C.; Swenson, D. *Nature* **1989**, *338* (6216), 594−596.
(75) Kaarsholm, N. C.; Ko, H. C.; Dunn, M. F. *Biochemistry* **1989**, *28* (10), 4427−4435.
(76) Smith, G. D.; Dodson, G. G. *Biopolym. Orig. Res. Biomol.* **1992**, *32* (4), 441−445.
(77) Choi, W. E.; Borchardt, D.; Kaarsholm, N. C.; Brzovic, P. S.; Dunn, M. F. *Proteins Struct. Funct. Bioinforma.* **1996**, *26* (4), 377−390.
(78) Jacoby, E.; KrüGer, P.; Karatas, Y.; Wollmer, A. *Biol. Chem. Hoppe. Seyler.* **1993**, *374* (7−12), 877−886.
(79) Maltesen, M. J.; Bjerregaard, S.; Hovgaard, L.; Havelund, S.; Van De Weert, M. *J. Pharm. Sci.* **2009**, *98* (9), 3265−3277.
(80) Ferrari, D.; Diers, J. R.; Bocian, D. F.; Kaarsholm, N. C.; Dunn, M. F. *Biopolym. - Biospectroscopy Sect.* **2001**, *62* (5), 249−260.
(81) Smith, G. D.; Ciszak, E.; Magrum, L. A.; Pangborn, W. A.; Blessing, R. H. *Acta Crystallogr. Sect. D Biol. Crystallogr.* **2000**, *56* (12), 1541−1548.
(82) Smith, G. D.; Pangborn, W. A.; Blessing, R. H. *Acta Crystallogr. Sect. D Biol. Crystallogr.* **2003**, *59* (3), 474−482.
(83) Smith, G. D.; Pangborn, W. A.; Blessing, R. H. *Acta Crystallogr. Sect. D Biol. Crystallogr.* **2001**, *57* (8), 1091−1100.
(84) Nakagawa, S. H.; Zhao, M.; Hua, Q.; Hu, S.-Q.; Wan, Z.; Jia, W.; Weiss, M. A. *Biochemistry* **2005**, *44* (13), 4984−4999.
(85) Weiss, M. A. *Vitam. Horm.* **2009**, *80*, 33−49.
(86) Vinther, T. N.; Norrman, M.; Ribel, U.; Huus, K.; Schlein, M.; Steensgaard, D. B.; Pedersen, T. Å.; Pettersson, I.; Ludvigsen, S.; Kjeldsen, T.; Jensen, K. J.; Hubálek, F. *Protein Sci.* **2013**, *22* (3), 296−305.
(87) Antoszewski, A.; Lorpaiboon, C.; Strahan, J.; Dinner, A. R. *J. Phys. Chem. B* **2021**, *125* (42), 11637−11649.
(88) Hassiepen, U.; Federwisch, M.; Mülders, T.; Wollmer, A. *Biophys. J.* **1999**, *77* (3), 1638−1654.
(89) Berchtold, H.; Hilgenfeld, R. *Biopolym. - Pept. Sci. Sect.* **1999**, *51* (2), 165−172.
(90) Ciszak, E.; Smith, G. D. *Biochemistry* **1994**, *33* (6), 1512−1517.
(91) Rahuel-Clermont, S.; French, C. A.; Kaarsholm, N. C.; Dunn, M. F. *Biochemistry* **1997**, *36* (19), 5837−5845.
(92) Vashisth, H.; Abrams, C. F. *Biophys. J.* **2008**, *95* (9), 4193−4204.
(93) Li, M.; Reichert, P.; Narasimhan, C.; Sorman, B.; Xu, W.; Cote, A.; Su, Y. *Mol. Pharmaceutics* **2022**, *19* (3), 936−952.

https://doi.org/10.1021/acs.analchem.3c04040
Anal. Chem. 2024, 96, 4756−4763

pubs.acs.org/ac

analytical chemistry

March 26, 2024 Volume 96 Number 12

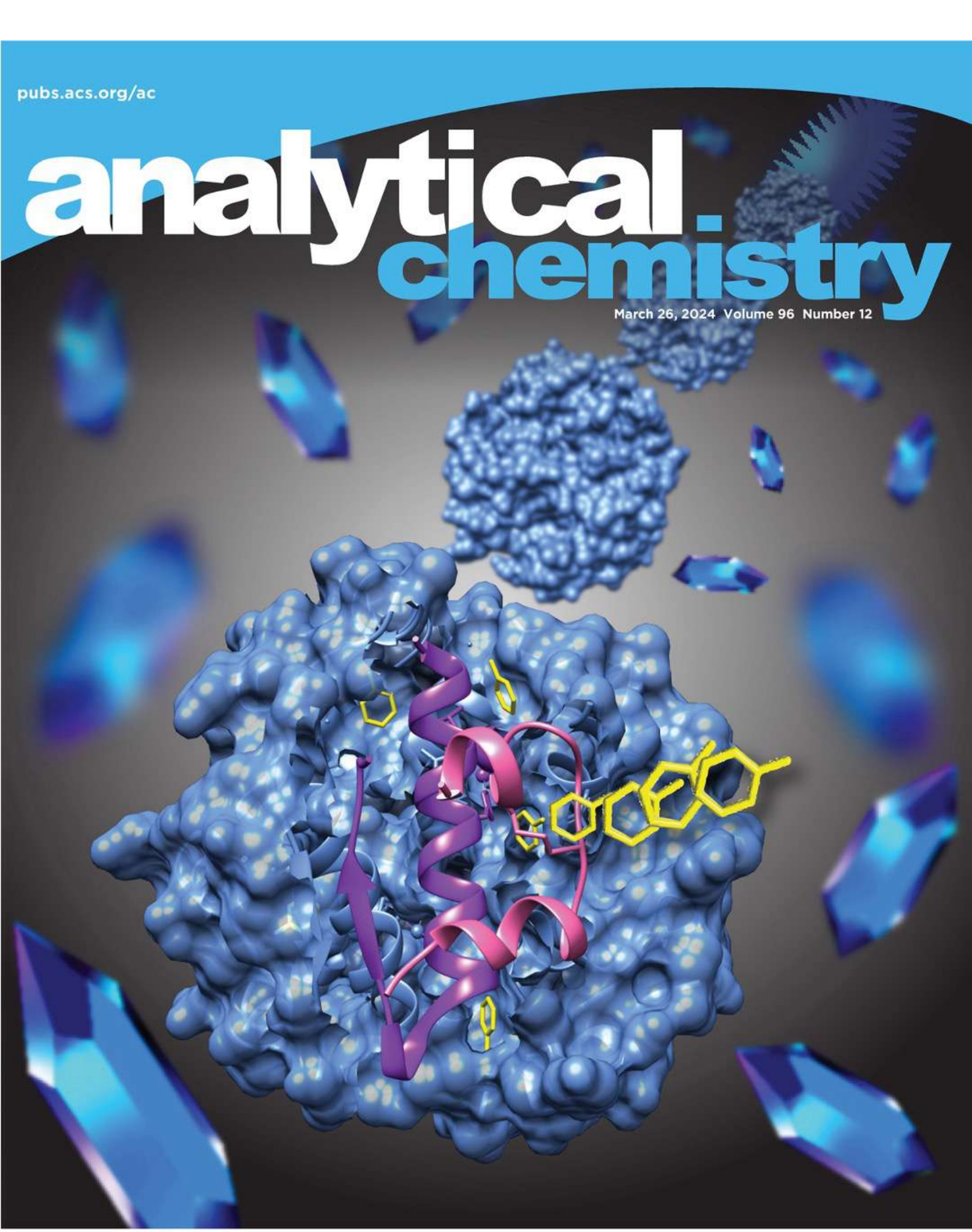

ACS Publications
Most Trusted. Most Cited. Most Read.

www.acs.org